Long-lasting Insecticidal Nets and the Quest for Malaria Eradication: A Mathematical Modeling Approach

Iboi Enahoro[†], Steffen Eikenberry[†], Abba B. Gumel[*†a], Silvie Huijben[‡] and Krijn Paaijmans[‡,‡‡]

[†]*School of Mathematical and Statistical Sciences, Arizona State University, Tempe, Arizona, USA.*

[‡]*Center for Evolution and Medicine & School of Life Sciences,*

[‡‡]*The Biodesign Center for Immunotherapy, Vaccines and Virotherapy,*

Arizona State University, Tempe, Arizona, USA.

[a] *Other affiliation: Department of Mathematics and Applied Mathematics,*

University of Pretoria, Pretoria 0002, South Africa.

March 18, 2020

Abstract

Recent dramatic declines in global malaria burden and mortality can be largely attributed to the large-scale deployment of insecticidal-based measures, namely long-lasting insecticidal nets (LLINs) and indoor residual spraying (IRS). However, the sustainability of these gains, and the feasibility of global malaria eradication by 2040, may be affected by increasing insecticide resistance among the *Anopheles* malaria vector. We employ a new differential-equations based mathematical model, which incorporates the full, weather-dependent mosquito lifecycle, to assess the population-level impact of the large-scale use of LLINs, under different levels of *Anopheles* pyrethroid insecticide resistance, on malaria transmission dynamics and control in a community. Moreover, we describe the bednet-mosquito interaction using parameters that can be estimated from the large experimental hut trial literature under varying levels of effective pyrethroid resistance. An expression for the basic reproduction number, $\mathcal{R}_0$, as a function of population-level bednet coverage, is derived. It is shown, owing to the phenomenon of backward bifurcation, that $\mathcal{R}_0$ must be pushed appreciably below 1 to eliminate malaria in endemic areas, potentially complicating eradication efforts. Numerical simulations of the model suggest that, when the baseline $\mathcal{R}_0$ is high (corresponding roughly to holoendemic malaria), very high bednet coverage with highly effective nets is necessary to approach conditions for malaria elimination. Further, while >50% bednet coverage is likely sufficient to strongly control or eliminate malaria from areas with a mesoendemic malaria baseline, pyrethroid resistance could undermine control and elimination efforts even in this setting. Our simulations show that pyrethroid resistance in mosquitoes

*Corresponding author: agumel@asu.edu

appreciably reduces bednet effectiveness across parameter space. This modeling study also suggests that increasing pre-bloodmeal deterrence of mosquitoes (deterring them from entry into protected homes) actually hampers elimination efforts, as it may focus mosquito biting onto a smaller unprotected host subpopulation. Finally, we observe that temperature affects malaria potential independently of bednet coverage and pyrethroid-resistance levels, with both climate change and pyrethroid resistance posing future threats to malaria control.

Keywords: Pyrethroid; LLINs; basic reproduction number; temperature effects.

1 Introduction

Malaria, a deadly disease caused by protozoan *Plasmodium* parasites that spread between humans via the bite of infected adult female *Anopheles* mosquitoes [124, 125], remains a major public health burden affecting many parts of the globe. Over 2.5 billion people live in areas whose local epidemiology permits transmission of *P. falciparum*, responsible for the most life-threatening form of malaria [50, 64]. The disease is endemic in 91 countries, and caused 219 million cases and 435,000 deaths in 2017 [22, 117, 130]. Disease burden is concentrated in the African Region, accounting for about 90% of cases and mortality (with the majority of deaths in children under the age of five) [125]. Other populations at high risk of malaria include pregnant women and those living with HIV/AIDS (owing to their weakened immune systems) [82, 124]. Malaria transmission dynamics is greatly affected by numerous abiotic and biotic factors, such as the increased mobility of people (the reservoir for the malaria parasite), the altered distribution of disease vectors (*Anopheles* mosquitoes) due to climate and environmental changes, and malaria's incursions into new areas (e.g., East African tropical highlands [57]).

The lifecycle of the ectothermal *Anopheles* mosquito, which consists of three aquatic juvenile stages (eggs, larva and pupa) and an adult stage, is intimately connected to local weather conditions [40, 96, 98], and is fundamental to the spread of malaria. In sub-Saharan Africa, favorable environmental conditions (a warm tropical climate) and the relatively long lifespans and strong human biting habits of the major local *Anopheles* species, along with broader socioeconomic conditions, and agricultural and land-use practices, make this region particularly vulnerable to malaria transmission. Adult female *Anopheles* mosquitoes take blood meals from vertebrate hosts (needed for egg development) every few days, with the exact interval depending strongly upon temperature [15]. The mosquito acquires *Plasmodium* infection by taking blood meals from an infected human, and subsequently passes the disease to a susceptible human, once parasite maturation within the mosquito is complete. As mosquitoes must routinely survive the time interval from initial infection to infectivity (which could range from 8 to 30 days, depending on ambient temperature [34]) for malaria to be transmitted, this explains why the relatively long lifespans of African *Anopheles* is so important for effective malaria transmission.

Great success has been recorded in the fight against malaria since about the year 2000, largely owing to concerted global public health efforts, such as the Roll Back Malaria initiative and the United Nations Millennium Development Goals (MDGs)[59, 123]. However, malaria remains a major public health challenge for about half of the world's population

[51, 121, 122]. New concerted global efforts, such as The Global Technical Strategy for Malaria 2016–2030 (approved by the World Health Assembly in May 2015 [123]) and the Zero by 40 Initiative (an initiative of five chemical companies with the support of the Bill & Melinda Gates Foundation and the Innovative Vector Control Consortium[117, 119]), aimed at eradicating malaria by 2030 or 2040, respectively, are currently underway. Central to these laudable malaria eradication efforts is the widespread use of insecticide-based vector control interventions, including pyrethroid-based insecticide-treated nets (ITNs; later replaced by long-lasting insecticidal nets (LLINs)), indoor residual spraying (IRS) and larvacides [10, 59, 95, 120], complemented by artemisinin-based combination drug therapy. Five major classes of insecticide are used in malaria control efforts, namely pyrethroids, organochlorines, organophosphates, carbamates and the recent addition of neonicotinoids, with all five used for IRS [129]. Only the pyrethroids, however, owing to their low mammalian toxicity and irritant effect on mosquitoes, are recommended for ITNs/LLINs [65]. It is notable that the earlier WHO's (World Health Organization's) Global Malaria Eradication Programme (1955–1969) relied almost exclusively on the use of DDT (*Dichlorodiphenyltrichloroethane*) and other insecticidal compounds for vector control, with the theoretical goal of interrupting malaria transmission via decreasing adult *survival times*, rather than decreasing mosquito abundance *per se*, a goal largely based on the mathematical model of the malariologist George Macdonald [77, 87]. Long-lasting insecticidal bednets have been used to great success in reducing the global malaria burden [16]. This success is partly attributed to community protection. In particular, if the coverage of bednet usage exceeds a certain threshold level, overall mosquito densities and malaria transmission are impacted sufficiently to also protect those individuals not using a bednet [67, 76, 95].

It has been estimated that bednets and IRS accounted for 81% of the reduction in malaria burden recorded in the past 15 years (with most of the benefits resulting from the use of bednets) [16]. The dramatic success of pyrethroid-based LLINs (over IRS) is likely due to multiple factors, including the fact that LLINs target indoor-biting mosquitoes, are effective as a physical barrier to biting, and pyrthroids have an excito-repellent effect that may diverting mosquitoes before they feed on the (protected) human host. However, at the most basic level, the success of LLINs is likely simply due to the enormous scale of implementation in endemic areas, especially in sub-Saharan Africa: Nearly 1.5 billion pyrethroid-based bednets have been deployed in endemic areas since 2010, with 1.25 billion distributed in sub-Saharan Africa [59, 111]. Unfortunately, this widespread and heavy use of insecticides has resulted in the emergence of vector resistance to nearly every currently-available agent used in the insecticides [3, 38, 62, 126] with pyrethroid resistance via multiple molecular mechanisms now widely observed across the African continent [55]. Given this, and the dominant role of LLINs in malaria mortality reductions, any threat to their efficacy via resistance is of foremost importance.

Perhaps most significantly, a recent and very large observational cohort study across five countries found that while LLIN users had lower rates of malaria infection and disease, no relationship between laboratory-assessed insecticide resistance and malaria epidemiology was detected [69]. Nevertheless, at least some data does suggest that resistance can undermine the control of malaria disease. One recent study suggests that insecticide resistance has led to a rebound in malaria incidence in South Africa [3]. A large, factorial randomized clinical trial [102] comparing LLINs, LLINs treated with a piperonyl butoxide (PBO) synergist, and

IRS, showed benefit to malaria control with either IRS or a PBO synergist in addition to an LLIN, suggesting that pyrethroid resistance decreased the efficacy of the standard LLIN alone. A recent experimental hut trial [113] also suggested benefit to LLINs with PBO synergists in an area with highly pythrethroid-resistant *Anopheles*.

Some prior mathematical work has examined the impact of insecticide resistance on malaria transmission dynamics. For example, Barbosa et al. [10] developed a genetic model to predict changes in mosquito fitness and resistance allele frequency (parameters that describe insecticide selection, fitness cost as well as LLINs and synergist (PBO) are incorporated). The results of their investigation suggested that resistance was most sensitive to selection coefficients, fitness cost and dominance coefficients. Chitnis et al. [28] developed and analysed a linear difference equation model for the dynamics of host-seeking adult female mosquitoes in a heterogeneous population of hosts in a community where ITNs are used. In addition to incorporating the gonotrophic cycle of the malaria vector and the aforementioned host heterogeneity, other notable features of the model in [28] include stage-structure in *Anopheles* feeding cycle and that such cycle varies across mosquitoes as well as allowing for the assessment of various mosquito control interventions. Consistent with previous studies for the impact of ITNs on malaria epidemiology in both ITN-protected and unprotect hosts, the Chitnis et al. study [28] shows beneficial effects to unprotected humans at both, low and high, ITN coverage levels. Birget et al. [17] developed a population-genetic model of the spread of insecticide-resistance in *Anopheles* mosquitoes in response to ITNs and larvicides, which suggested indoor ITNs were less likely to select for resistance. Brown et al. [21] developed a mathematical model to investigate optimal (cost-effective) strategies for mosquito control in the presence of insecticide resistance. Consistent with previous studies, their results show that fitness costs are the key elements in the computation of economically optimal resistance management strategies. Mohammed-Awel et al. [83] designed a novel deterministic model for assessing the population-level impact of mosquito insecticide resistance on malaria transmission dynamics and to evaluate the community-wide impact of the use ITNs, IRS and their combination. Their study showed that the prospect of the effective control of malaria spread in endemic settings (while minimizing the risk of insecticide resistance in the female adult mosquito population), using ITNs and IRS, is quite promising (provided the effectiveness and coverage levels are at optimal levels). Birget and Koella [18] proposed a model to assess the relative importance in different epidemiological contexts of repellent and insecticidal properties of ITNs. Gu and Novak [118] used an agent-based model that incorporated the killing and avoidance of individual mosquitoes exposed to ITNs in a hypothetical village setting with 50 houses and 90 aquatic habitats. Smith et al. [109] used a mathematical model to establish the relationship between *P. falciparum* parasite rate (*PfPR*) and ITNs coverage. Killeen and Smith [67] proposed a model that describes the interaction of a blood-seeking mosquito with either bednet-protected or unprotected hosts as a two-stage process, whereby mosquito are either diverted from the attempt, or engage in an attempt and then either die or succeed in taking a bloodmeal. Similar bednet-human interaction and feeding cycle models are described in [53, 68, 79, 97].

The main objective of the current study has been to develop a mathematical model for assessing the impact of insecticide resistance on malaria epidemiology in malaria-endemic areas that adopt wide-scale use of LLINs. The main motivation is twofold. First is the fact that LLINs are the core intervention (due to their superior success over IRS) for National

Malaria Prevention Programs [127, 128]. Second is the fact that the impact of pyrethroid resistance on malaria transmission/epidemiology is not well-understood and remains a subject for considerable debate within the malaria control community [3, 69, 102, 113]. The developed model, which takes the form of a deterministic system of nonlinear differential equations, incorporates key features of aquatic and adult mosquito dynamics (including the aquatic developmental stages, adult mosquito gonotrophic cycle, parasite sporogony and schizogony in the hosts population), disease transmission in humans, and the use of bednets as the sole control strategy. The human population is stratified based on whether or not they use LLINs. We partly adapt the prior weather-dependent malaria model of Okuneye et al. [96], and previous bednet-mosquito interaction models, such as those proposed in [53, 67, 68, 79, 97]. We have reviewed the experimental hut trial literature, and the relationships between key parameters describing bednet efficacy have been extracted from a large number of experimental studies. Thus, the model quantitatively represents resistance in a realistic manner.

The ultimate goal is to determine whether effective disease control (or elimination) is feasible, using LLINs, despite insecticide resistance. The paper is organized as follows. The model is formulated in Section 2, and analysed for its qualitative features in Section 3. The effect of local temperature variability on the effectiveness of LLINs (and, hence, on disease dynamics and control) is assessed in Section 4. Discussion and concluding remarks are reported in Section 5.

2 Model Formulation

The model describes the temporal dynamics of immature and adult mosquitoes and humans. The total immature mosquito population is split into compartments for eggs ($E(t)$), four larval instar stages ($L_i(t)$; $i = 1, 2, 3, 4$ and pupae ($P(t)$). The dynamics of the adult female mosquitoes is governed by the gonotrophic cycle. Following [96], the adult female mosquito gonotrophic cycle is divided into three stages [32, 96]:

Stage I : host-seeking and taking of a bloodmeal

Stage II : digestion of bloodmeal and egg maturation

Stage III : search for, and oviposition into, a suitable body of water (breeding site)

The populations of vectors in Stages I, II and III of the gonotrophic cycle at time t are denoted by $X(t)$, $Y(t)$ and $Z(t)$, respectively. With respect to *Plasmodium* infection and the sporogonic cycle, vectors in each gonotrophic stage is further subdivided into susceptible ($S_X(t), S_Y(t), S_Z(t)$), exposed (i.e., infected but not yet infectious) ($E_X(t), E_Y(t), E_Z(t)$) and infectious ($I_X(t), I_Y(t), I_Z(t)$) compartments. Thus, the total number of adult female *Anopheles* mosquitoes at time t, denoted by $N_M(t)$, is given by

$$N_M(t) = S_X(t) + E_X(t) + I_X(t) + S_Y(t) + E_Y(t) + I_Y(t) + S_Z(t) + E_Z(t) + I_Z(t).$$

The total human population at time t, denoted by $N_H(t)$, is split into the total number of humans who are protected by bednets (i.e., those who consistently sleep under an LLIN),

denoted by $N_{H_p}(t)$, and those who are not protected, denoted by $N_{H_u}(t)$. The population of protected and unprotected individuals is further subdivided into susceptible $S_{H_p}(t)(S_{H_u}(t))$, exposed $E_{H_p}(t)(E_{H_u}(t))$, infectious $I_{H_p}(t)(I_{H_u}(t))$ and recovered $R_{H_p}(t)(R_{H_u}(t))$ humans, so that

$$\begin{aligned} N_H(t) &= N_{Hp}(t) + N_{Hu}(t), \\ &= S_{H_p}(t) + S_{H_u}(t) + E_{H_p}(t) + E_{H_u}(t) + I_{H_p}(t) + I_{H_u}(t) + R_{H_p}(t) + R_{H_u}(t). \end{aligned}$$

The flow diagram of the model to be developed is depicted in Figure 1.

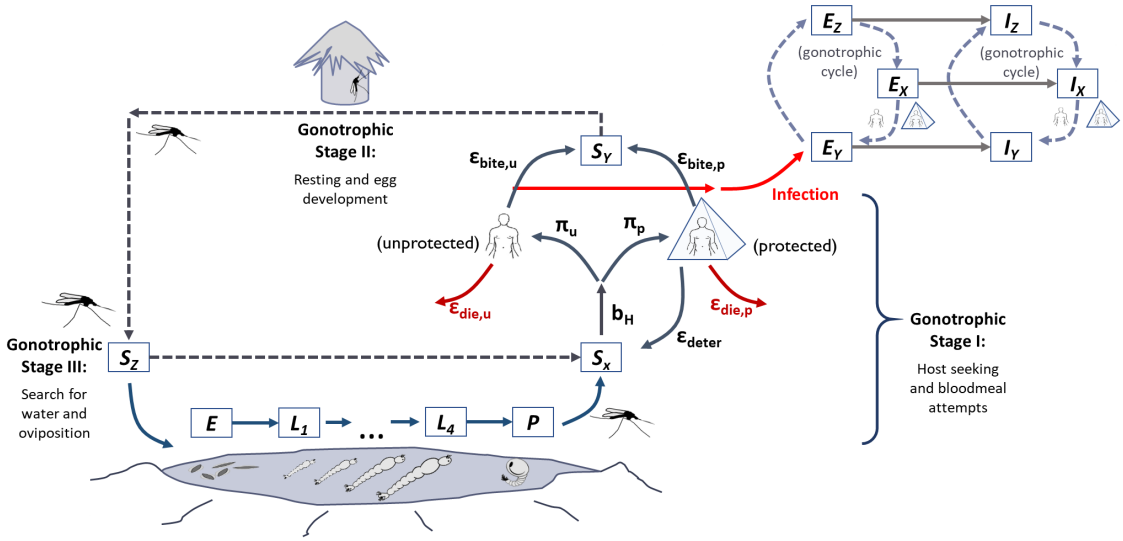

Figure 1: Flow diagram of the model {(2.1), (2.2), (2.4)}.

2.1 Equations for the Dynamics of Immature Mosquitoes

It is convenient to define $L = \sum_{j=1}^{4} L_j$. The equations for the dynamics of immature mosquitoes are given by (where a dot represents differentiation with respect to time t):

$$\begin{aligned} \dot{E} &= \psi_E \varphi_Z \left(1 - \frac{E}{K_E}\right)_+ (S_Z + E_Z + I_Z) - [\sigma_E(T_W) + \mu_E(T_W)]E, \\ \dot{L}_1 &= \sigma_E(T_W)E - [\sigma_{L_1}(T_W) + \mu_L(T_W) + \delta_L L]L_1, \\ \dot{L}_j &= \sigma_{Lj-1}(T_W)L_{j-1} - [\sigma_{L_j}(T_W) + \mu_L(T_W) + \delta_L L]L_j;\ j = 2,3,4, \\ \dot{P} &= \sigma_{L_4}(T_W)L_4 - [\sigma_P(T_W) + \mu_P(T_W)]P, \end{aligned} \tag{2.1}$$

where T_A and T_W represent air and water, temperature, respectively. In (2.1), ψ_E is the number of eggs laid *per* oviposition, φ_Z is the rate at which female mosquitoes transition from Stage III to Stage I of the gonotrophic cycle (i.e., the rate of oviposition for

mosquitoes in Stage III) and K_E is the environmental carrying capacity of eggs (the notation $r_+ = \max\{0, r\}$ is used to ensure the non-negativity of the logistic term). The quantity $\delta_L L$ represents the density-dependent larval mortality rate [1]. Further, μ_i and σ_i $(i = E, L, P)$ represent the natural death and maturation rates of immature mosquitoes of type i, respectively. The temperature-dependence of the developmental and survival parameters is presented in Section 2.4.

2.2 Equations for the Dynamics of Adult Female *Anopheles* Mosquitoes

As stated above, the dynamics of the adult female *Anopheles* mosquitoes is governed by the gonotrophic cycle. The total vector population is split into the aforementioned nine compartments $(S_X, E_X, I_X, S_Y, E_Y, I_Y, S_Z, E_Z, I_Z)$ corresponding to the three gonotrophic cycle stages [96]. We let π_p represent the proportion of humans that are protected by a bednet (i.e. consistently sleep under an LLIN), while $\pi_u = 1 - \pi_p$ is the unprotected portion. In other words, $0 < \pi_p \leq 1$ is the bednet coverage. Bednet-mosquito interactions are defined by three basic parameters: ε_{deter}, $\varepsilon_{die,i}$, and $\varepsilon_{bite,i}$, as described now. We let ε_{deter} represent the **probability** that an adult female mosquito is deterred from entering an LLIN-protected hut (or house), relative to an unprotected hut (or house). That is,

$$\varepsilon_{\text{deter}} = \frac{\text{Number of mosquitoes in control group} - \text{Number of mosquitoes in the protected hut}}{\text{Number of mosquitoes in the control group}}.$$

It should be emphasized that, in the context of this study, "deterrence" (as measured by the parameter ε_{deter}) means that the mosquito is deterred from entering the house before any attempt is made to take a bloodmeal. Thus, the parameter ε_{deter} does not include any direct "barrier" property of the net.

We let $\varepsilon_{die,i}$ (with $i = \{p, u\}$; p=protected; u=unprotected) represent the probability that an adult female mosquito dies following entry into a protected (unprotected) house. The parameters $\varepsilon_{bite|die,i}$ and $\varepsilon_{bite|\sim die,i}$ represent, respectively, the probability that an adult female mosquito successfully takes a bloodmeal from the human host, given that the mosquito did or did not die, with i (p or u) indicating the bednet protection status of the targeted human Figure 2 depicts the associated decision tree of the aforementioned probabilities).

The (temperature-dependent) equations for adult female mosquito dynamics are given by:

$$\text{Stage I} \begin{cases} \dot{S}_X &= f\sigma_P(T_W)P + \varphi_Z S_Z + b_H(Q_2 + Q_3)S_X - [b_H Q_1 + \mu_{\mathbf{X}} + \mu_M(T_A)]S_X, \\ \dot{E}_X &= \varphi_Z E_Z + b_H(Q_2 + Q_3)E_X - [b_H Q_1 + \kappa_V(T_A) + \mu_{\mathbf{X}} + \mu_M(T_A)]E_X, \\ \dot{I}_X &= \varphi_Z I_Z + \kappa_V(T_A)E_X + b_H(Q_2 + Q_3)I_X - [b_H Q_1 + \mu_{\mathbf{X}} + \mu_M(T_A)]I_X, \end{cases} \tag{2.2}$$

$$\text{Stage II} \begin{cases} \dot{S}_Y &= b_H[(1 - \beta_V\omega_p)R_1 + (1 - \beta_V\omega_u)R_2]S_X - [\theta_Y(T_A) + \mu_M(T_A)]S_Y, \\ \dot{E}_Y &= b_H(\beta_V\omega_p R_1 + \beta_V\omega_u R_2)S_X + b_H(R_1 + R_2)E_X - [\theta_Y(T_A) + \kappa_V(T_A) + \mu_M(T_A)]E_Y, \\ \dot{I}_Y &= \kappa_V(T_A)E_Y + b_H(R_1 + R_2)I_X - [\theta_Y(T_A) + \mu_M(T_A)]I_Y, \end{cases}$$

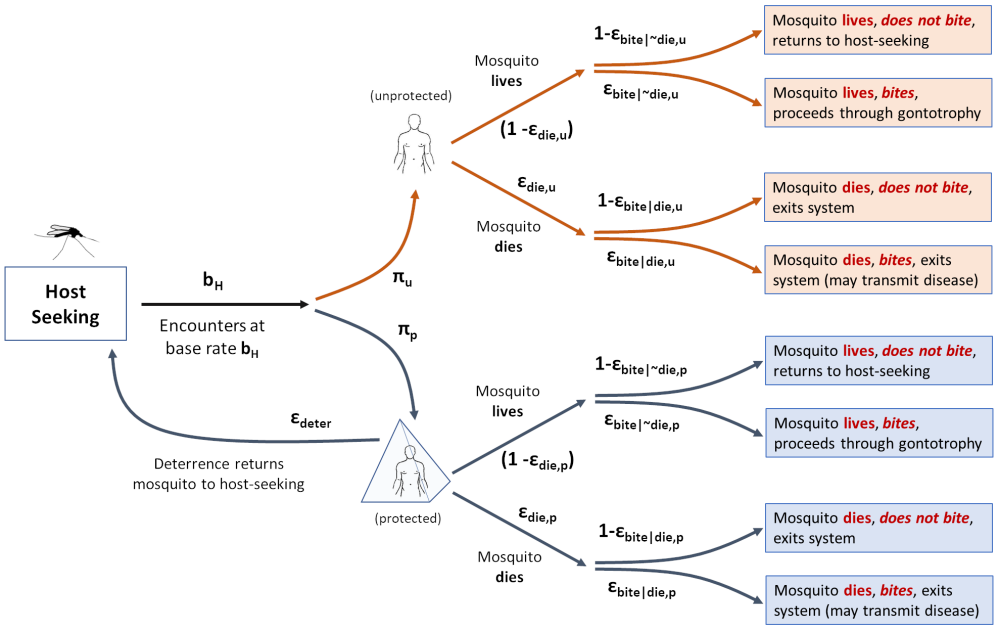

Figure 2: A decision tree of probabilities of the model {(2.1), (2.2), (2.4)}.

$$\text{Stage III}\begin{cases}\dot{S}_Z &= \theta_Y(T_A)S_Y - [\varphi_Z + \mu_M(T_A)]S_Z,\\ \dot{E}_Z &= \theta_Y(T_A)E_Y - [\varphi_Z + \kappa_V(T_A) + \mu_M(T_A)]E_Z,\\ \dot{I}_Z &= \theta_Y(T_A)I_Y + \kappa_V(T_A)E_Z - [\varphi_Z + \mu_M(T_A)]I_Z.\end{cases}$$

where,

$$\begin{aligned} Q_1 &= \pi_p(1-\varepsilon_{deter}) + \pi_u,\\ Q_2 &= \pi_p(1-\varepsilon_{deter})(1-\varepsilon_{die,p})(1-\varepsilon_{bite|\sim die,p}),\\ Q_3 &= \pi_u(1-\varepsilon_{die,u})(1-\varepsilon_{bite|\sim die,u}),\\ R_1 &= \pi_p(1-\varepsilon_{deter})(1-\varepsilon_{die,p})\varepsilon_{bite|\sim die,p},\\ R_2 &= \pi_u(1-\varepsilon_{die,u})\varepsilon_{bite|\sim die,u},\\ \omega_p &= \frac{I_{H_p}}{N_{H_p}},\\ \omega_u &= \frac{I_{H_u}}{N_{H_u}}, \end{aligned} \tag{2.3}$$

with ω_p (ω_u) representing the fractions of protected (unprotected) humans that are infectious.

In (2.2) and (2.2), the term $f\sigma_P$ $(0 < f < 1)$ represents the proportion of new adult mosquitoes that are females. Susceptible adult mosquitoes in Stage I of the gonotrophic cycle encounter hosts at a rate $b_H Q_1$ (where b_H is the mosquito-host encounter rate per unit time, and Q_1 is defined above). The rate $b_H(Q_2 + Q_3)$ represents failure to take a bloodmeal ending in survival (and thus a return to stage I of the gonotrophic cycle), while $b_H(R_1 + R_2)$ is the rate at which encounters result in successful bloodmeals and survival. It should be emphasized that, in the formulation of the model (2.2) questing adult female mosquitoes that do not succeed in biting bednet-protected humans will not necessarily have

to bite an unprotected human. They will simply look for a bloodmeal from another human who may be protected or not (see Figure 1). The parameter κ_V represents the maturation rate of malaria parasite in the mosquito (i.e., $\frac{1}{\kappa_V}$ is the average duration of the sporogonic cycle), while the parameter θ_Y is the progression rate from Stage II to Stage III of the gonotrophic cycle. Susceptible adult female mosquitoes in Stage II of the gonotrophic cycle acquire malaria infection at the rate $b_H(\beta_V\omega_p R_1 + \beta_V\omega_u R_2)$, where β_V is the transmission probability from infectious human to a susceptible mosquito, ω_p and ω_u are the fractions of protected and unprotected infectious humans, respectively, and μ_M is the natural mortality rate of adult female mosquitoes. **Following Chitnis** *et al.* **[28], we assume an additional mortality rate, μ_X, for adult female mosquitoes in the host-seeking stage, as this stage of the gonotrophic cycle is expected to be most hazardous to the adult female mosquitoes. Moreover, this helps account for a survival cost potentially incurred when the adult female mosquitoes are deterred from protected hosts and, thus, must expend more energy in questing for bloodmeal. Furthermore, as noted by Cator** *et al.* **[31], sporozoite-infected** *Anopheles gambiae* **females are more likely than uninfected females to take bloodmeal from multiple hosts in the same night, and they suffer higher feeding-associated mortality. It should, however, be mentioned that very little is known about adult mosquito mortality in the field, and the degree that mortality is associated with bloodfeeding events is unknown. Such data, when available, will be very valuable in malaria modeling studies**.

From the above formulation, the (time-varying) entomological inoculation rates (EIRs; the average numbers of infectious bites per human per unit time [40]) for protected and unprotected hosts are given, respectively, by

$$\begin{aligned}
\mathrm{EIR}_p(t) &= b_H \frac{I_X(t)}{N_{H_p}(t)} \pi_p (1-\varepsilon_{deter}) \left[\varepsilon_{bite|die,p}\, \varepsilon_{die,p} + \varepsilon_{bite|\sim die,p}(1-\varepsilon_{die,p})\right], \\
\mathrm{EIR}_u(t) &= b_H \frac{I_X(t)}{N_{H_u}(t)} \pi_u \left[\varepsilon_{bite|die,u}\, \varepsilon_{die,u} + \varepsilon_{bite|\sim die,u}(1-\varepsilon_{die,u})\right].
\end{aligned}$$

Similarly, the biting (infectious or uninfectious) rates for protected and unprotected host are given, respectively, by

$$\begin{aligned}
\mathrm{biting}_p(t) &= b_H \frac{[S_X(t)+E_X(t)+I_X(t)]}{N_{H_p}(t)} \pi_p (1-\varepsilon_{deter}) \left[\varepsilon_{bite|die,p}\, \varepsilon_{die,p} + \varepsilon_{bite|\sim die,p}(1-\varepsilon_{die,p})\right], \\
\mathrm{biting}_u(t) &= b_H \frac{[S_X(t)+E_X(t)+I_X(t)]}{N_{H_u}(t)} \pi_u \left[\varepsilon_{bite|die,u}\, \varepsilon_{die,u} + \varepsilon_{bite|\sim die,u}(1-\varepsilon_{die,u})\right].
\end{aligned}$$

The parameters related to the use of LLINs in the community (i.e., b_H, π_p, π_u, ε_{deter}, $\varepsilon_{bite|\sim die,p}$, $\varepsilon_{bite|\sim die,u}$, $\varepsilon_{bite|die,p}$, $\varepsilon_{bite|die,u}$, $\varepsilon_{die,p}$ and $\varepsilon_{die,u}$) have been estimated for various mosquito-bednet pairings using experimental hut trial data conducted in various parts of sub-Saharan Africa. We assume, for this work, that $\varepsilon_{bite|\sim die,i} = \varepsilon_{bite,i}$, for $i = u, p$. In brief, such trials typically include a control net and several treated nets that may be of different classes (conventional ITN vs. LLIN), subject to different degrees of wear (e.g. washing and/or artificial holing), and conducted in areas with different levels of local anopheline

pyrethroid resistance (or employ lab strains). Volunteers sleep under nets in these trials, and the total number of mosquitoes collected in each hut, the total bloodfed, and the total dead are typically reported. We identified 26 publications conducted in Africa that reported sufficient detail to calculate the above metrics [6, 7, 8, 11, 22, 27, 32, 33, 35, 36, 42, 66, 70, 72, 80, 81, 89, 90, 91, 92, 93, 94, 99, 100, 103, 114],

Every mosquito-hut pairing reported in these trials gives a value for $\varepsilon_{die,p}$, $\varepsilon_{bite,p}$, and ε_{deter}. Moreover, each pairing represents some "effective" level of insecticide resistance (i.e. an ineffective net and a sensitive mosquito and effective net but highly resistant mosquito may both represent pairings of high effective resistance). These pairings can be used to estimate how $\varepsilon_{die,p}$ and $\varepsilon_{bite,p}$ systematically co-vary as effective resistance changes, and a functional relationship between $\varepsilon_{die,p}$ (the probability of death following encounter with a protected host) and $\varepsilon_{bite,p}$ (the probability of taking a bloodmeal from a protected host) can been estimated, as depicted in Figure 3. We choose the exponential relation,

$$\varepsilon_{bite,p} = a_0 \exp\left(-b_0 \, \varepsilon_{die,p}\right),$$

where the best-fit values of the constants a_0 and b_0 are found, using weighted nonlinear least squares (weighting by number of mosquitoes collected in each trial), to be $a_0 = 0.55$ and $b_0 = 2$. The value of this relationship is that it allows effective bednet resistance to be described by a single parameter, $\varepsilon_{die,p}$, with $\varepsilon_{bite,p}$ determined as a function of $\varepsilon_{die,p}$. Following Randriamaherijaona et al. [103], we estimate the probability that a mosquito takes a bloodmeal from a person sleeping without a net or under an extremely holed untreated net is on the order of 70-80%, while the probability of death is $\leq 5\%$. Hence, we take $\varepsilon_{bite,u} = 0.7$ and $\varepsilon_{die,u} = 0.05$ as baseline parameters for encounters with unprotected hosts. The parameter ε_{deter} is assumed to vary between 0.01 to 0.4.

In this study, the following three effectiveness levels of the LLINs are considered (given in Table 4), as also highlighted in Figure 3:

(i) Weakly-effective net: this is a net that has low killing efficacy and high biting probability. For this setting, we choose $\varepsilon_{die,p} = 0.25, \varepsilon_{bite,p} = 0.33$. Here, the adult mosquitoes are highly resistant to the net.

(ii) Moderately-effective net: this is a net with moderate killing efficacy and moderate biting probability. Here, we set $\varepsilon_{die,p} = 0.5, \varepsilon_{bite,p} = 0.2$, and the adult mosquitoes are moderately resistant to the net.

(iii) Highly-effective net: this is a net with very high killing efficacy and very low biting probability. Here, we set $\varepsilon_{die,p} = 0.9, \varepsilon_{bite,p} = 0.1$. This corresponds to the case where the adult mosquitoes are weakly resistant to the net.

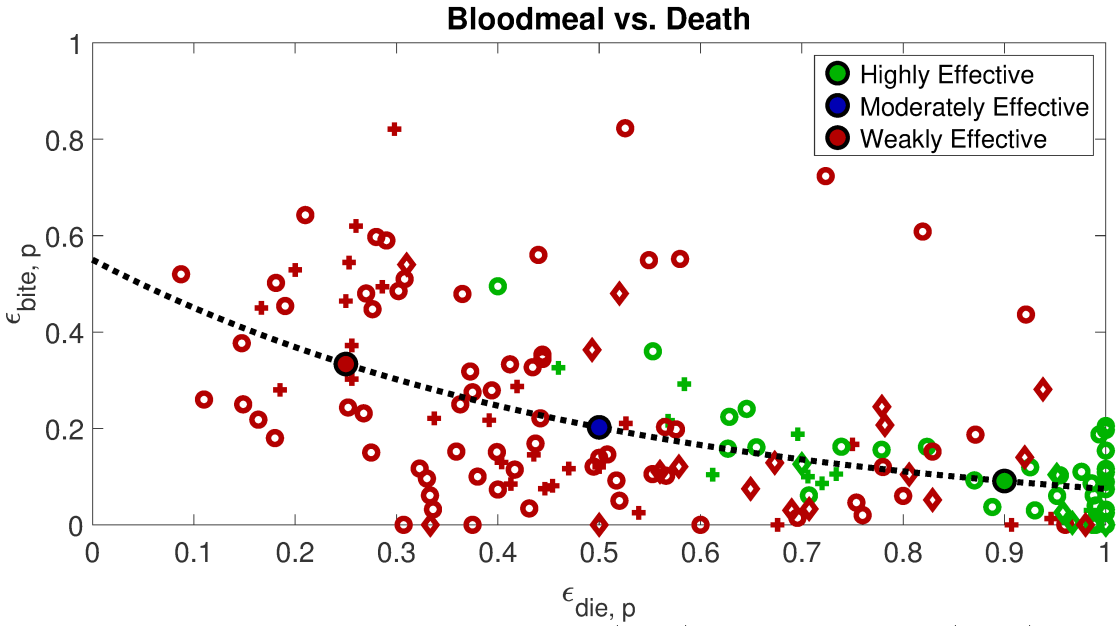

Figure 3: Data-points showing probability of death ($\varepsilon_{die,p}$) and blood feeding ($\varepsilon_{bite,p}$) for various mosquito-net pairings drawn from experimental hut trial data. Each point is coded according to net type by symbol shape, and according to mosquito resistance class (either pyrethroid resistant or sensitive). Additionally, representative points on the exponential curve fit relating $\varepsilon_{bite,p}$ to $\varepsilon_{die,p}$ are marked, signifying parameters for a **highly effective** ($\varepsilon_{die,p} = 0.9$, $\varepsilon_{bite,p} = 0.1$), **moderately effective** ($\varepsilon_{die,p} = 0.5$, $\varepsilon_{bite,p} = 0.2$), and **weakly effective** ($\varepsilon_{die,p} = 0.25$, $\varepsilon_{bite,p} = 0.33$) bednet. Data for the curves is drawn from the references [6, 7, 8, 11, 22, 27, 32, 33, 35, 36, 42, 66, 70, 72, 80, 81, 89, 90, 91, 92, 93, 94, 99, 100, 103, 114], as described further in the text.

2.3 Equations for the Dynamics of Human Population

The equations for the dynamics of the human population are given by:

$$\begin{aligned}
\dot{S}_{H_p} &= \Pi\,\pi_p + \eta_H R_{H_p} - (\lambda_{VH_p} + \mu_H) S_{H_p}, \\
\dot{E}_{H_p} &= \lambda_{VH_p} S_{H_p} - (\gamma_H + \mu_H) E_{H_p}, \\
\dot{I}_{H_p} &= \gamma_H E_{H_p} - (\alpha_H + \mu_H + \delta_H) I_{H_p}, \\
\dot{R}_{H_p} &= \alpha_H I_{H_p} - (\eta_H + \mu_H) R_{H_p}, \\
\dot{S}_{H_u} &= \Pi\,\pi_u + \eta_H R_{H_u} - (\lambda_{VH_u} + \mu_H) S_{H_u}, \\
\dot{E}_{H_u} &= \lambda_{VH_u} S_{H_u} - (\gamma_H + \mu_H) E_{H_u}, \\
\dot{I}_{H_u} &= \gamma_H E_{H_u} - (\alpha_H + \mu_H + \delta_H) I_{H_u}, \\
\dot{R}_{H_u} &= \alpha_H I_{H_u} - (\eta_H + \mu_H) R_{H_u},
\end{aligned} \tag{2.4}$$

where, $\lambda_{VH_p}(t) = \beta_M \,\mathrm{EIR}_p(t)$ and $\lambda_{VH_u}(t) = \beta_M \,\mathrm{EIR}_u(t)$.

In (2.4), Π represents the recruitment rate of individuals (by birth or immigration) into the population (with π_p and π_u as defined in Section 2). The parameter η_H represents the loss of immunity by individuals who recovered from malaria. Susceptible protected humans acquire malaria infection from infectious mosquitoes at a rate $\lambda_{VHp}\,(\lambda_{VHu})$, with β_M being the probability of infection *per* bite and EIR_p (EIR_u) as defined in Section 2. Natural mortality occurs in all human compartments at a rate μ_H. Infected individuals develop clinical symptoms of malaria at a rate γ_H, and recover at a rate α_H. Finally malaria-induced death occurs in the infectious human population at a rate δ_H.

The model {(2.1), (2.2), (2.4)} is a modification of the model in [96] by:

(a) explicitly including the dynamics of the adult mosquitoes under the influence of bednet usage (in Stages I and II of the gonotrophic cycle);

(b) stratifying the human population in terms of bednets usage (only one class for susceptible, exposed, infectious and recovered humans was used in [96]).

The 23-dimensional nonlinear continuous-time model {(2.1), (2.2), (2.4)} is also an extension of the 3-dimenisonal, linear, difference equation model developed by Chitnis *et al.* [28] by:

(i) explicitly including the dynamics of the immature mosquitoes (i.e., adding equations for the dynamics of eggs, the four larval instars and the pupal stages of the aquatic cycle; this was not included in [28]) ;

(ii) explicitly incorporating the deterrence property of the bednet (this was not explicitly included in [28]);

(iii) explicitly including the dynamics of the adult mosquitoes under the influence of bednet usage (in Stages I and II of the gonotrophic cycle);

(iv) including the dynamics of humans *vis a vis* malaria transmission, and stratifying the human population in terms of bednets usage (the dynamics of humans is not explicitly incorporated in the model in [28], making the model linear);

(v) explicitly incorporating the effect of temperature variability on the population ecology of immature and adult mosquitoes (this was not considered in [28]).

Furthermore, unlike in the case of the model in [28], the model developed in this study is simulated subject to three effectiveness levels (low, moderate and high) of the bednets used in the community. This allows for the assessment of various levels of insecticide resistance in the community (these bednets effectiveness levels are not considered in [28]).

The state variables and parameters of the model {(2.1), (2.2), (2.4)} are described in Tables 1-3. Baseline values and ranges of the parameters of the model are tabulated in Table 4 (more detailed descriptions may be found in [96]). All bednet-related parameters vary with net effectiveness, as described above, with the sole exception of ε_{deter}, which we fix at 0.1 for all simulation results, unless otherwise stated.

Table 1: Description of state variables for the model {(2.1), (2.2), (2.4)}

Variables	**Interpretation**
E	Number of eggs
L_j $(j = 1, 2, 3, 4)$	Number of larvae at instar Stage j
P	Number of pupae
S_X, E_X, I_X	Number of susceptible, exposed, and infectious female mosquitoes in gonotrophic Stage I, respectively
S_Y, E_Y, I_Y	Number of susceptible, exposed, and infectious female mosquitoes in gonotrophic Stage II, respectively
S_Z, E_Z, I_Z	Number of susceptible, exposed, and infectious, female mosquitoes in gonotrophic Stage III, respectively
$S_{H_p}(S_{H_u})$	Number of protected (unprotected) susceptible humans
$E_{H_p}(E_{H_u})$	Number of protected (unprotected) exposed (infected but not yet infectious) humans
$I_{H_p}(I_{H_u})$	Number of protected (unprotected) infectious (symptomatic) humans
$R_{H_p}(R_{H_u})$	Number of protected (unprotected) recovered humans

2.4 Temperature-dependent Parameters

Both vector and parasite are ectothermal (dependent on ambient temperature). Thus, their life histories are significantly affected by temperature. For instance, adult and immature aquatic mosquito survival is maximized for temperature values in the mid-20s (°C), with survival tailing off rather symetrically at higher and lower temperatures [40]. Further, the development rates of *Plasmodium* parasites, immature anophelines and mosquito eggs generally increase with increasing temperature to, at least, about 30°C [98, 40]. Thermal response functions for temperature-dependent parameters are determined from experimental lab data as follows.

Death rate of adult female mosquitoes ($\mu_M(T_A)$). The mean survival times for adult *Anopheles gambiae* under laboratory conditions, and under constant ambient temperatures ranging from 5 to 40°C (5 °C intervals), are taken from [12].

$$\frac{1}{\mu_M(T_A)} = \max(0.01, a + bT_A + cT_A^2), \tag{2.5}$$

Table 2: Description of bednet-independent parameters of the model {(2.1), (2.2), (2.4)}

Parameters	Interpretation
μ_M	Mortality rate for the mosquito population
μ_X	**Additional mortality rate for those mosquitoes deterred from entering the protected hut**
δ_L	Density-dependent mortality rate of larvae
κ_V	Progression rate of exposed adult female mosquito to infectious stage
φ_Z	Oviposition rate for adult in Stage III of the gonotrophic cycle (Stage III to Stage I transition)
β_V	Transmission probability from infected human to a susceptible mosquito
β_M	Transmission probability from infected mosquito to a susceptible human
$\omega_p(\omega_u)$	Fraction of protected (unprotected) humans that are infectious
θ_Y	Progression rate for Stage II of the gonotrophic cycle
f	Proportion of adult mosquitoes that are females
ψ_E	Number of eggs per oviposition event (Stage III to Stage I transition)
K_E	Carrying capacity of eggs
σ_E	Maturation rate from egg to larvae
σ_L	Maturation rate from larvae to pupae
σ_P	Maturation rate from pupae to adult mosquitoes
μ_E	Mortality rate of eggs
μ_L	Mortality rate of larvae
μ_P	Mortality rate of pupae
Π	Recruitment rate of humans into the population
λ_{VH}	Infection rate of susceptible humans
γ_H	Progression rate of humans from exposed to infectious (symptomatic) class
δ_H	Malaria-induced mortality rate for humans
α_H	Recovery rate of infected humans
η_H	Rate of loss of infection-acquired immunity
μ_H	Natural mortality rate of humans

Table 3: Description of bednet-related parameters of the model {(2.1), (2.2), (2.4)}

Parameters	Interpretation
π_p	Proportion of protected hosts
π_u	Proportion of unprotected hosts
ε_{deter}	Probability repelled before entering protected hut relative to unprotected
$\varepsilon_{bite\|\sim die,p}$	Probability of bloodmeal in protected houses
$\varepsilon_{bite\|\sim die,u}$	Probability of bloodmeal in unprotected houses
$\varepsilon_{bite\|die,p}$	Probability of bloodmeal, given death, in protected houses
$\varepsilon_{bite\|die,u}$	Probability of bloodmeal, given death, in unprotected houses
$\varepsilon_{die,p}$	Probability of death in protected houses
$\varepsilon_{die,u}$	Probability of death in unprotected houses

Table 4: Parameters for bednet effectiveness levels with deterrence ϵ_{deter} set to zero.

Bednet effectiveness	$\varepsilon_{die,p}$	$\varepsilon_{bite,p}$
Weakly-effective net	0.25	0.33
Moderately-effective net	0.5	0.2
Highly-effective net	0.9	0.1

Table 5: Ranges and baseline values of temperature-independent parameters of the model {(2.1), (2.2), (2.4)}. The estimate for K_E is defined in terms of the total human population at the disease-free equilibrium ($\frac{\Pi}{\mu_H}$) to ensure that the mosquito: host ratio falls within the realistic range of 0.1 to 10 mosquitoes *per* person *per* day typically encountered in the field [77].

Parameters	Range (per day)	Baseline Value (per day)	Reference
μ_M	0.0431—0.1000	0.0431	Adapted from [96]
μ_X	**0—0.1**	**0.05**	**Estimated**
δ_L	0—0.0001	0.00002	Adapted from [96]
κ_V	0.070—0.0973	0.0851	Adapted from [96]
β_V	0.0200—0.2500 (dimensionless)	0.1500 (dimensionless)	[25, 73]
β_M	0.0100—0.5000 (dimensionless)	0.5000 (dimensionless)	[106, 108]
θ_Y	0.4000—0.4964	0.2807	Adapted from [96]
f	0.5000—0.8000 (dimensionless)	0.5000 (dimensionless)	[96]
ψ_E	10—150 eggs per oviposition	65	[110]
φ_Z	0.5000—4.000	2.000	[34]
K_E	1.0×10^4—1.0×10^6	$100 \times \frac{\Pi}{\mu_H}$	[96]
σ_E	0.3300—1.0000	0.4499	[116]
σ_{L_j} $(j = 1, 2, 3, 4)$	0.3599—0.5399	0.4499	Adapted from [96]
σ_P	0.3300—1.0000	0.4499	[13]
μ_E	0.0608—0.0912	0.0760	Adapted from [96]
μ_L	0.0608—0.0912	0.0760	Adapted from [96]
μ_P	0.0608—0.0912	0.0760	Adapted from [96]
Π	4.000—5.5000 humans	4.5000	[96]
γ_H	1/17—1/14	1/14	[96]
δ_H	0.0001–0.0030	0.0021	[2, 37, 105, 96]
α_H	1/1500—1/100	1/30	[9, 63, 96, 107]
η_H	$1/(3 \times 365) - 1/(7 \times 365)$	$1/(3 \times 365)$	[44]
μ_H	$1/(50 \times 365) - 1/(70 \times 365)$	$1/(60 \times 365)$	[96]

where a = -11.8239, b = 3.3292 and c = -0.0771.

Transition rate from Stage II to Stage III of gonotrophic cycle ($\theta_Y(T_A)$). We describe the rate at which mosquitoes complete Stage II of the gonotrophic cycle (that is, the transition from the Y to Z compartment(s)), using a Briere function [20], such that

$$\theta_Y(T_A) = cT_A(T_A - T_A^0)(T_A^m - T_A)^{\frac{1}{2}}, \tag{2.6}$$

and parameter values are adopted from Mordecai et al. [84], with $c = 0.000203$, $T_A^m = 42.3$°C and $T_A^0 = 11.7$°C .

Sporogony ($\kappa(T_A)$). We follow Paaijmans et al. [98] and use a Briere function for $\kappa(T_A)$, given by the right-hand side of (2.6) with parameters $c = 0.000112$, $T_A^m = 35$°C , and $T_A^0 = 15.384$°C .

Death rate of immature mosquitoes ($\mu_E(T_W)$, $\mu_L(T_W)$, $\mu_P(T_W)$). We assume that temperature-dependent death rates are equal for eggs, larvae, and pupae, and use laboratory larval survival times reported by Bayoh and Lindsay [14], to fit a *per-capita* death rate (inverse of survival time) with the fourth-order polynomial,

$$\mu_i(T_W) = 8.929\times10^{-6}T_W^4 - 0.0009271T_W^3 + 0.03536T_W^2 - 0.5814T_W + 3.509, i = E, L, P. \tag{2.7}$$

Development rate of immature mosquitoes ($\sigma_E(T_W)$, $\sigma_L(T_W)$, $\sigma_P(T_W)$). We adopt the relationship between water temperature and overall time from egg to adult, $l(T_W)$, given by Bayoh and Lindsay [13] (based on laboratory data),

$$l(T_W) = (a + bT_W + ce^{T_W} + de^{-T_W})^{-1}, \tag{2.8}$$

with $a = -0.05$, b = 0.005, c = -2.139×10^{-16} and $d = -281357.656$. We assume that the duration of all six immature stages (egg, four larval instars, and pupa) is equal, giving [96]. We determined stage-specific development times as a function of temperature from Figure 1 of Bayoh and Lindsay [13], as shown in Figure 4. Development times are similar across all immature stages, with appreciable overlap in the temperature-dependent curves. Therefore, we simply assume all stages have the same duration, and the uniform temperature-dependent development rates are given as

$$\sigma_E(T_W) = \sigma_P(T_W) = \sigma_L(T_W) = 6\frac{1}{l(T_W)}. \tag{2.9}$$

We have assumed, for this study, that near the surface of the water, air and water temperature are approximately equal [1, 60], giving $T_A = T_W$ (unless otherwise stated, a default value of $T_A = T_W = 25$ °C will be used to compute each of the aforementioned temperature-dependent parameters of the model). Further, since (by using fixed temperature values) the aforementioned temperature-dependent parameters take constant values, the model {(2.1), (2.2), (2.4)} is *autonomous*. This assumption is made for mathematical tractability.

2.5 Basic Qualitative Properties of the Model

The basic qualitative properties of the model {(2.1), (2.2), (2.4)} in the absence of density-dependent mortality rate in the larvae stage ($\delta_L = 0$) are explored in this section, with the positivity and boundedness of the solutions of the model established.

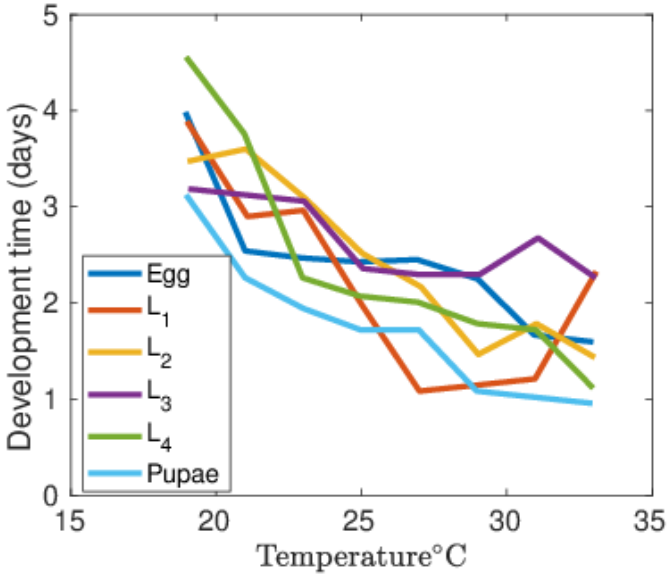

Figure 4: Development times of the dynamics of the immature mosquitoes.

Let $A_X = S_X + E_X + I_X$, $A_Y = S_Y + E_Y + I_Y$, $A_Z = S_Z + E_Z + I_Z$ and $N_M(t) = A_X(t) + A_Y(t) + A_Z(t)$. Further, define

$$\mathcal{X} = \big(E, L_1, L_2, L_3, L_4, P, S_X, E_X, I_X, S_Y, E_Y, I_Y, S_Z, E_Z, I_Z, S_{H_p}, E_{H_p}, I_{H_p}, R_{H_u}, S_{H_u}, E_{H_u}, I_{H_u}, R_{H_u}\big)\,.$$

It is convenient to group the variables of the model $\{(2.1), (2.2), (2.4)\}$ as follows:

$$\begin{aligned} \mathcal{B}_1 &= (E, L_1, L_2, L_3, L_4, P)\,, \\ \mathcal{B}_2 &= (S_X, E_X, I_X, S_Y, E_Y, I_Y, S_Z, E_Z, I_Z)\,, \\ \mathcal{B}_3 &= \big(S_{H_p}, E_{H_p}, I_{H_p}, R_{H_u}, S_{H_u}, E_{H_u}, I_{H_u}, R_{H_u}\big)\,. \end{aligned} \tag{2.10}$$

Consider the feasible region $\Omega = \Omega_1 \times \Omega_2 \times \Omega_3$ for the model $\{(2.1), (2.2), (2.4)\}$, where:

$$\begin{aligned} \Omega_1 &= \left\{\mathcal{B}_1 \in \mathbb{R}^6_+ : E(t) \leq K_E, L_1(t) \leq L_1^\diamond, L_2(t) \leq L_2^\diamond, L_3(t) \leq L_3^\diamond, L_4(t) \leq L_4^\diamond, P(t) \leq P^\diamond\right\}, \\ \Omega_2 &= \left\{\mathcal{B}_2 \in \mathbb{R}^9_+ : N_M(t) \leq \tfrac{f\sigma_P P^\diamond}{\mu_M}\right\},\ \Omega_3 = \left\{\mathcal{B}_3 \in \mathbb{R}^8_+ : N_H(t) \leq \tfrac{\Pi}{\mu_H}\right\}, \end{aligned} \tag{2.11}$$

with, $L_1^\diamond = \frac{\sigma_E K_E}{\sigma_{L_1}+\mu_L}$, $L_2^\diamond = \frac{\sigma_{L_1} L_1^\diamond}{\sigma_{L_2}+\mu_L}$, $L_3^\diamond = \frac{\sigma_{L_2} L_2^\diamond}{\sigma_{L_3}+\mu_L}$, $L_4^\diamond = \frac{\sigma_{L_3} L_3^\diamond}{\sigma_{L_4}+\mu_L}$ and $P^\diamond = \frac{\sigma_{L_4} L_4^\diamond}{\sigma_P+\mu_P}$.
We claim the following result.

Lemma 2.1 *Consider the model $\{(2.1), (2.2), (2.4)\}$.*

(a) Each component of the solution of the model, with non-negative initial conditions, remains positive and bounded for all time $t > 0$.

(b) The set Ω is positively-invariant and attracting region for the model.

The proof of Lemma 2.1 is given in Appendix A.

3 Mathematical Analysis

In this section, the model {(2.1), (2.2), (2.4)} is rigorously analysed to show the existence and asymptotic stability of its disease-free equilibrium, and to characterize the bifurcation structure of the model. We define the threshold quantity, $\mathcal{N}_0$, as

$$\mathcal{N}_0 = \frac{\psi_E \varphi_Z \sigma_E f \sigma_P \theta_Y C_2 \prod_{i=1}^{4} \sigma_{L_i}}{(C_1 K_9 K_{11} - C_2 \theta_Y \varphi_Z) \prod_{i=1}^{6} K_i}, \tag{3.1}$$

where $\mathbf{C_1 = K_7 - b_H(Q_2 + Q_3)}$, $C_2 = b_H(R_1 + R_2)$, $K_1 = \sigma_E + \mu_E$, $K_j = \sigma_{L_{j-1}} + \mu_L$ $(j = 2, ..., 5)$, $K_6 = \sigma_P + \mu_P$, $\mathbf{K_7 = b_H Q_1 + \mu_X + \mu_M}$, $K_9 = \theta_Y + \mu_M$ and $K_{11} = \varphi_Z + \mu_M$. Furthermore (noting the definitions of C_9, C_{10} and C_{11} given in Appendix B), $C_1 K_9 K_{11} - C_2 \theta_Y \varphi_Z = \mu_M^3 + \mu_M^2 C_9 + \mu_M C_{10} + C_{11} > 0$. Hence, $\mathcal{N}_0 > 0$.

The quantity $\mathcal{N}_0$, which is the *extinction threshold* for the mosquito population of the model, measures the average number of new adult female mosquitoes produced by one reproductive mosquito during its entire reproductive period [40, 96].

3.1 Existence of the Disease-free Equilibrium

The existence and asymptotic stability of the disease-free equilibrium (DFE) of the model {(2.1), (2.2), (2.4)} is demonstrated here, and we examine the following equilibria:

(i) The model {(2.1), (2.2), (2.4)} has a trivial disease-free equilibrium (*TDFE*), given by:

$$\begin{aligned}\mathcal{T}_1 &= \left(0,0,0,0,0,0,0,0,0,0,0,0,0,0,0,0,S^*_{H_p},0,0,0,S^*_{H_u},0,0,0\right),\\ &= \left(0,0,0,0,0,0,0,0,0,0,0,0,0,0,0,0,\frac{\Pi\,\pi_p}{\mu_H},0,0,0,\frac{\Pi\,\pi_u}{\mu_H},0,0,0\right).\end{aligned}$$

The equilibrium $\mathcal{T}_1$ is ecologically unrealistic (since it is associated with the total absence of mosquitoes in the community). Hence, it is not analysed.

(ii) The model {(2.1), (2.2), (2.4)} has a unique non-trivial disease-free equilibrium (*NDFE*), given by:

$$\mathcal{T}_2 = \left(E^*, L_1^*, L_2^*, L_3^*, L_4^*, P^*, S_X^*, 0, 0, S_Y^*, 0, 0, S_Z^*, 0, 0, \frac{\Pi\,\pi_p}{\mu_H}, 0, 0, 0, \frac{\Pi\,\pi_u}{\mu_H}, 0, 0, 0\right),$$

where,

$$\begin{aligned}&E^* = K_E\left(1 - \frac{1}{\mathcal{N}_0}\right),\ L_1^* = \frac{\sigma_E E^*}{K_2},\ L_2^* = \frac{\sigma_{L_1} L_1^*}{K_3},\ L_3^* = \frac{\sigma_{L_2} L_2^*}{K_4},\\ &L_4^* = \frac{\sigma_{L_3} L_3^*}{K_5},\ P^* = \frac{\sigma_{L_4} L_4^*}{K_6},\ S_X^* = \frac{\left[f\sigma_E\sigma_P K_E\left(1 - \frac{1}{\mathcal{N}_0}\right) K_9 K_{11}\right] \prod_{i=1}^{4} \sigma_{L_i}}{(C_1 K_9 K_{11} - C_2\theta_Y\varphi_Z) \prod_{i=2}^{6} K_i},\\ &S_Y^* = \frac{C_2 S_X^*}{K_9},\ S_Z^* = \frac{\theta_Y S_Y^*}{K_{11}}.\end{aligned} \tag{3.2}$$

It is clear from Equation (3.2) that the equilibrium $\mathcal{T}_2$ exists if and only if $\mathcal{N}_0 > 1$ (it is assumed from here on that $\mathcal{N}_0 > 1$, so that the non-trivial disease-free equilibrium, $\mathcal{T}_2$, exists). It is worth noting that the *NDFE* ($\mathcal{T}_2$) is the non-extinction equilibrium for the mosquito population coupled with the trivial disease-free equilibrium ($\mathcal{T}_1$) for the human population. Hence, in the absence of the vectors and the disease, the two subsystems ($\mathcal{T}_1$ and $\mathcal{T}_2$) are uncoupled.

3.2 Asymptotic Stability of the NDFE

Consider the model {(2.1), (2.2), (2.4)}. It can be shown, using the next generation operator method [115], that the associated reproduction number $\mathcal{R}_0$ of the model is given by:

$$\mathcal{R}_0 = \sqrt{(\mathcal{R}_{H_pV} + \mathcal{R}_{H_uV}) \times \mathcal{R}_{VH}}, \tag{3.3}$$

where,

$$\mathcal{R}_{H_pV} = \frac{\gamma_H \beta_V N^*_{Hu} Q_p R_1}{K_{13} K_{14}}, \ \mathcal{R}_{H_uV} = \frac{\gamma_H \beta_V N^*_{Hp} Q_u R_2}{K_{13} K_{14}}, \tag{3.4}$$

and,

$$\mathcal{R}_{VH} = \frac{b_H \beta_M S^*_X}{N^*_{Hp} N^*_{Hu}} \frac{\kappa_V \varphi_Z \theta_Y [(K_9 + K_{12}) C_3 + K_9 K_{11}]}{(C_3 K_{10} K_{12} - C_2 \theta_Y \varphi_Z)(C_1 K_9 K_{11} - C_2 \theta_Y \varphi_Z)}, \tag{3.5}$$

with,

$$\begin{aligned} Q_p &= b_H \pi_p (1 - \varepsilon_{deter}) \left[\varepsilon_{bite|die,p} \, \epsilon_{die,p} + \varepsilon_{bite|\sim die,p} (1 - \varepsilon_{die,p}) \right], \\ Q_u &= b_H \pi_u \left[\varepsilon_{bite|die,u} \, \varepsilon_{die,u} + \varepsilon_{bite|\sim die,u} (1 - \varepsilon_{die,u}) \right], \end{aligned}$$

$N^*_{Hp} = \frac{\Pi \pi_p}{\mu_H}$, $N^*_{Hu} = \frac{\Pi \pi_u}{\mu_H}$, $\mathbf{C_3 = K_8 - b_H(Q_2 + Q_3)}$, $\mathbf{K_8 = b_H Q_1 + \kappa_V + \mu_X + \mu_M}$, $K_{10} = \theta_Y + \kappa_V + \mu_M$, $K_{12} = \varphi_Z + \kappa_V + \mu_M$, $K_{13} = \gamma_H + \mu_H$ and $K_{14} = \alpha_H + \delta_H + \mu_H$. It can be shown that $C_3 K_{10} K_{12} - C_2 \theta_Y \varphi_Z = b_H [C_4 \kappa_V^2 + 2\kappa_V \left(\mu_M + \frac{\theta_Y}{2} + \frac{\varphi_Z}{2}\right) C_5 + C_6 + C_7] + C_8 > 0$ (where the coefficients $C_i \, (i = 2, ..., 8)$ are constants, and are given in Appendix D). Hence, $\mathcal{R}_{VH} > 0$ (and thus $\mathcal{R}_0$ is also automatically positive).

Theorem 3.1 *Let $\mathcal{N}_0 > 1$. The NDFE, $\mathcal{T}_2$, of the model {(2.1), (2.2), (2.4)} is locally-asymptotically stable (LAS) in $\Omega \setminus \mathcal{T}_1$ if $\mathcal{R}_0 < 1$, and unstable if $\mathcal{R}_0 > 1$.*

The epidemiological implication of Theorem 3.1 is that malaria is eliminated from the population if the initial sizes of the subpopulations of the model {(2.1), (2.2), (2.4)} are in the basin of attraction of the non-trivial disease-free equilibrium ($\mathcal{T}_2$). Hence, a small influx of malaria-infected individuals into the community will not generate large outbreaks, though larger influxes may.

It is notable that the value of the reproduction number ($\mathcal{R}_0$) for the worst-case scenario (i.e., bednet coverage is zero), denoted by $\tilde{\mathcal{R}}_{0*}$ and computed using the baseline parameter values in Table 4, is $\tilde{\mathcal{R}}_{0*} \simeq \mathbf{11.4}$ (see Appendix C for the formulation of the special case of the model {(2.1), (2.2),(2.4)} with no bednet coverage). This high value of the reproduction

number is typically seen in holo-endemic malaria regions [49]. It should be mentioned that, for the computation of the value of the reproduction number for this (holo-endemic) setting, we assumed (in Table 4) that there are, on average, 100 eggs per human (which translates to about 10 adult mosquitoes per human). When we reduce the number of eggs per human to 10 per human, so that we have one mosquito per human (which is more typically the case in meso-endemic regions [49]), the value of $\mathcal{R}_0$ reduces to $\tilde{\mathcal{R}}_{0*} \simeq \mathbf{3.6}$. Hence, these computations (together with Theorem 3.1) show that, for the worst-case scenario (with no bednets used in the community), the disease will persist in both the holoendemic and the mesoendemic regions (since $\tilde{\mathcal{R}}_{0*} > 1$ in both cases), as expected.

3.3 Existence of Backward Bifurcation

The phenomenon of backward bifurcation has been observed in numerous models (such as those in [19, 43, 45, 46, 60, 61]) for spread of malaria and other vector-borne diseases that incorporated disease-induced death in the host population. A backward bifurcation is characterized by the co-existence of two asymptotically-stable equilibria when $\mathcal{R}_0 < 1$: an endemic equilibrium point (EEP) and a disease-free equilibrium point (DFE). Thus, the classical epidemiological requirement that $\mathcal{R}_0$ be less than one for elimination of the disease, while necessary, is no longer sufficient to eliminate malaria when it already exists in the population. That is, while $\mathcal{R}_0 \geq 1$ remains a condition for malaria to spread within a previously unexposed population, pushing $\mathcal{R}_0 < 1$ via control measures does not necessarily guarantee elimination of the disease.

Theorem 3.2 *The model {(2.1), (2.2), (2.4)} undergoes a backward bifurcation at $\mathcal{R}_0 = 1$ whenever a bifurcation coefficient, denoted by a (given in Appendix D), is positive.*

Proof. The proof of Theorem 3.2, based on using Center Manifold theory [23, 24], is given in Appendix D. The result given by Theorem 3.2 is numerically illustrated by simulating the model {(2.1), (2.2), (2.4)} using parameter values such that the backward bifurcation condition, given in Appendix D, is satisfied (Figure 5).

The range for backward bifurcation for a **weakly-effective net** (i.e., a net with $\varepsilon_{die,p} = 0.25$, $\varepsilon_{bite,p} = 0.33$) is $\beta_M \in (0.526394, \infty)$, a **moderately-effective net** (i.e., a net with $\varepsilon_{die,p} = 0.5$, $\varepsilon_{bite,p} = 0.2$) is $\beta_M \in (0.503682, \infty)$ and that for a **highly- effective net** (i.e., a net with $\varepsilon_{die,p} = 0.9$, $\varepsilon_{bite,p} = 0.1$) is $\beta_M \in (1.4009823, \infty)$, where β_M is the chosen backward bifurcation parameter (see Appendix D). Hence, this study shows that the phenomenon of backward bifurcation is more likely to occur using a moderately-effective net than when either a weak or highly-effective net is used.

Theorem 3.2 shows that elimination is dependent on the initial sizes of the infected vector and human populations. For elimination to be independent of the size of the infected populations, a global asymptotic stability property must be explored for the non-trivial disease-free equilibrium ($\mathcal{T}_2$). **It is convenient to define the associated reproduction number of the model {(2.1), (2.2), (2.4)} in the absence of disease-induced mortality in the host population (δ_H) by**

$$\tilde{\mathcal{R}}_0 = \mathcal{R}_0|_{\delta_H=0}. \tag{3.6}$$

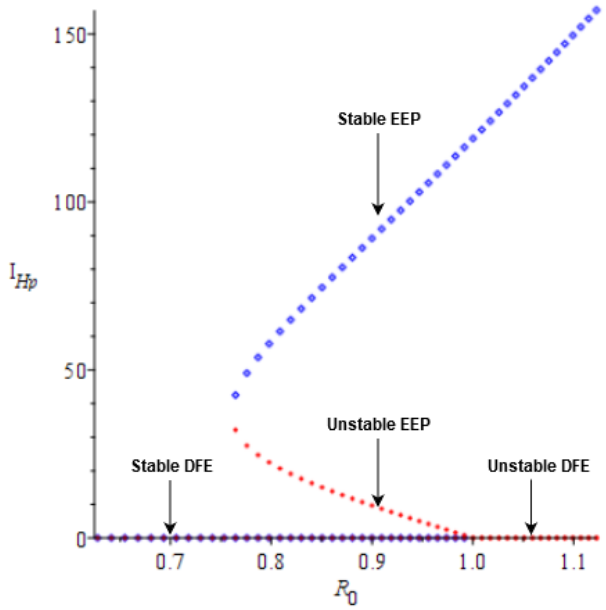

Figure 5: Backward bifurcation diagram of the model {(2.1), (2.2), (2.4)}, showing a plot of $I_{Hp}(t)$ as a function of the reproduction number $\mathcal{R}_0$, where β_M is the chosen bifurcation parameter. Parameter values used are as given in Table 5 with: $\pi_p = 0.5, \pi_u = 0.5, \varepsilon_{deter} = 0.75, \varepsilon_{bite|\sim die,p} = 0.1, \varepsilon_{bite|\sim die,u} = 0.7, \varepsilon_{bite|die,p} = 0.1, \varepsilon_{bite|die,u} = 0.7, \varepsilon_{die,p} = 0.9, \varepsilon_{die,u} = 0.05, b_H = 2, \mu_{\mathbf{X}} = \mathbf{0.005}, \psi_E = 5, \delta_H = 0.0005, \eta_H = 1/14, \beta_V = 0.5, \Pi = 1$ and $K_E = \frac{\Pi}{\mu_H}$ (so that the bifurcation coefficient, a (defined in Appendix D), is given by a=5.42 $\times 10^{-6} > 0$ and $\mathcal{R}_0 = 1$). It should be mentioned that in order to generate this figure, the values of seven parameters ($\mu_X, \psi_E, K_E, \eta_H, \delta_H, \beta_V$ and Π) have to be chosen outside their biologically-feasible ranges given in Table 5.

We claim the following.

Theorem 3.3 *The NDFE, $\mathcal{T}_2$, of the model {(2.1), (2.2), (2.4)}, with $\delta_H = 0$ and $\mathcal{N}_0 > 1$, is globally-asymptotically stable (GAS) in $\Omega \setminus \mathcal{T}_1$ if $\tilde{\mathcal{R}}_0 < 1$.*

The proof of Theorem 3.3, based on using Lyapunov function theory and LaSalle's Invariance Principle, is given in Appendix E. The epidemiological implication of Theorem 3.3 is that, for the special case of the model {(2.1), (2.2), (2.4)} with no disease-induced mortality in the host population (i.e., $\delta_H = 0$), bringing and maintaining the associated reproduction threshold ($\tilde{\mathcal{R}}_0$) to a value less than one is necessary and sufficient for complete elimination of malaria in the community, regardless of initial conditions.

4 Numerical Simulations: Populations at Equilibrium

4.1 Interaction between bednet coverage and bednet efficacy parameters

To assess the population-level impact of bednets on malaria transmission dynamics in the community under equilibrium conditions (i.e., the model is numerically simulated until an endemic equilibrium is reached), the model {(2.1), (2.2), (2.4)} is simulated using various bednet coverage and effectiveness levels, where bednet effectiveness is jointly defined by $\varepsilon_{bite,p}$ and $\varepsilon_{die,p}$. Unless otherwise stated, all simulations use the baseline parameter values in Table 5, and temperature is fixed at 25°C (i.e., the values of all the temperature-dependent parameters of the model are obtained by evaluating each of the functional forms in Section 2 at the fixed temperature T=25°C). Figure 6 illustrates the nonlinear relationships between bednet coverage fraction, π_p, disease prevalence in the two human populations (bednet-protected and unprotected), $\tilde{\mathcal{R}}_0$ (i.e., $\mathcal{R}_0$ for the case when the disease-induced mortality in the human population, δ_H, is set to zero), and EIR (again, in the bednet-protected and unprotected populations), at endemic equilibrium and for baseline parameters. Notably, this figure shows that EIR decreases with increasing bednet coverage (top right panel). This result is consistent with that reported in the modeling study by Chitnis et al. [28], which used data relevant to malaria transmission dynamics in Ifakara, Tanzania (i.e., data for *Anopheles gambiae* feeding on a heterogenous human population, with no cattle), to show that bednets are effective in reducing malaria transmission. Our result is also consistent with the results of the field trials on *permethrin*-treated bednets in western Kenya reported by Hawley et al. [54].

Further, as evident from the graph in the lower left panel of Figure 6, human disease prevalence varies hyperbolically with EIR (i.e., prevalence increases with increasing EIR), such that, for a high baseline EIR, a large reduction in EIR is required before any meaningful malaria control is realized. A five-fold reduction in overall EIR, however, is achieved with roughly 20% bednet coverage (see upper right panel of Figure 6). Thus, although even a relatively low bednet coverage can aid somewhat in malaria control, the simulations in Figure 6 show that much higher bednet coverage (and a decrease in EIR of two orders of magnitude) is needed to achieve malaria elimination. Finally, there is a similar, although

less marked, hyperbolic relationship between increasing $\tilde{\mathcal{R}}_0$ and increasing disease prevalence (bottom right panel).

We explore how changes in $\varepsilon_{bite,p}$ and $\varepsilon_{die,p}$ (i.e. net effectiveness) affect $\tilde{\mathcal{R}}_0$, starting from either a baseline $\tilde{\mathcal{R}}_0$ value of **11.7**, presumably representing holoendemic malaria, or **3.7**, which is more appropriate for mesoendemic malaria. In particular, we generate contour plots of $\tilde{\mathcal{R}}_0$ as a function of $\varepsilon_{bite,p}$ and $\varepsilon_{die,p}$, for either low (20%) or high (80%) bednet coverage levels (Figure 7). The inscribed curve on each contour plot of Figure 7 shows how $\varepsilon_{bite,p}$ and $\varepsilon_{die,p}$ co-vary, based upon the experimental hut data discussed in Section 2.2. In these plots, the highlighted points indicate highly, moderately, and weakly effective nets. It follows from Figure 7 that, for the mesoendemic baseline, even a moderately effective net is capable of pushing $\tilde{\mathcal{R}}_0$ to a value less than one when bednet coverage is high (80%). Further, for this (mesoendemic baseline scenario) even low bednet coverage (20%) may substantially improve malaria control. In the holoendemic baseline, on the other hand, only a highly effective net with high coverage can have a chance to approach malaria elimination. Thus, these simulations show that our study only supports the claim in the malaria modeling study by Chitnis et al. [28] (based on data relevant to malaria dynamics in Ifakara, Tanzania) and the *permethrin*-treated bednets field trial in western Kenya by Hawley et al. [54] that bednets reduce malaria transmission if the malaria region being considered is mesoendemic. For holoendemic malaria regions, our study shows that only a highly-effective net, coupled with very high coverage, can lead to effective control of malaria. Ifakara and western Kenya are considered regions of high malaria endemicity [52, 58].

Figure 7 also suggests that high coverage of weakly effective (i.e. low killing efficiency) nets is better than low coverage with highly effective (i.e. high killing efficiency) nets. For example, in the holoendemic setting, 20% coverage with a highly effective net pushe $\tilde{\mathcal{R}}_0$ from 11.7 to 5.5, while 80% coverage with a weakly effective net gives $\tilde{\mathcal{R}}_0$ of 3.6. Given the nonlinear relationship between $\tilde{\mathcal{R}}_0$ and disease prevalence, widespread use of even marginally effective bednets may better control malaria than lower coverage rates with better (more effective) nets.

Finally, Figure 8 shows the nonlinear relationship between $\tilde{\mathcal{R}}_0$ and EIR, such that EIR must be pushed very close to zero before $\tilde{\mathcal{R}}_0$ drops below one. In other words, Figure 8 shows that a significant reduction in EIR is needed in order to bring the reproduction number $\tilde{\mathcal{R}}_0$ to a value less than 1 (so that, by Theorem 3.3, malaria elimination can be achieved).

We also examine how deterrence, as measured in the model by ε_{deter}, interacts with bednet coverage and net effectiveness to determine $\tilde{\mathcal{R}}_0$, as shown in the contour plots in Figure 9. Perhaps surprisingly, increasing deterrence generally results in an *increase* in $\tilde{\mathcal{R}}_0$. This is likely because increasing ε_{deter} focuses mosquito biting upon the unprotected subpopulation, resulting in more intense malaria transmission among this subpopulation and an overall increase in $\tilde{\mathcal{R}}_0$. It should be emphasized here that this increased biting on unprotected persons is not an assumption directly imposed on the model, but is a natural consequence of the fact that, if a mosquito does not attempt a bloodmeal on a net-protected human she has encountered, due to deterrence, she will continue in her search and likely ultimately encounter an unprotected person (although this comes at an increased mortality, denoted by μ_X in the model 2.2).

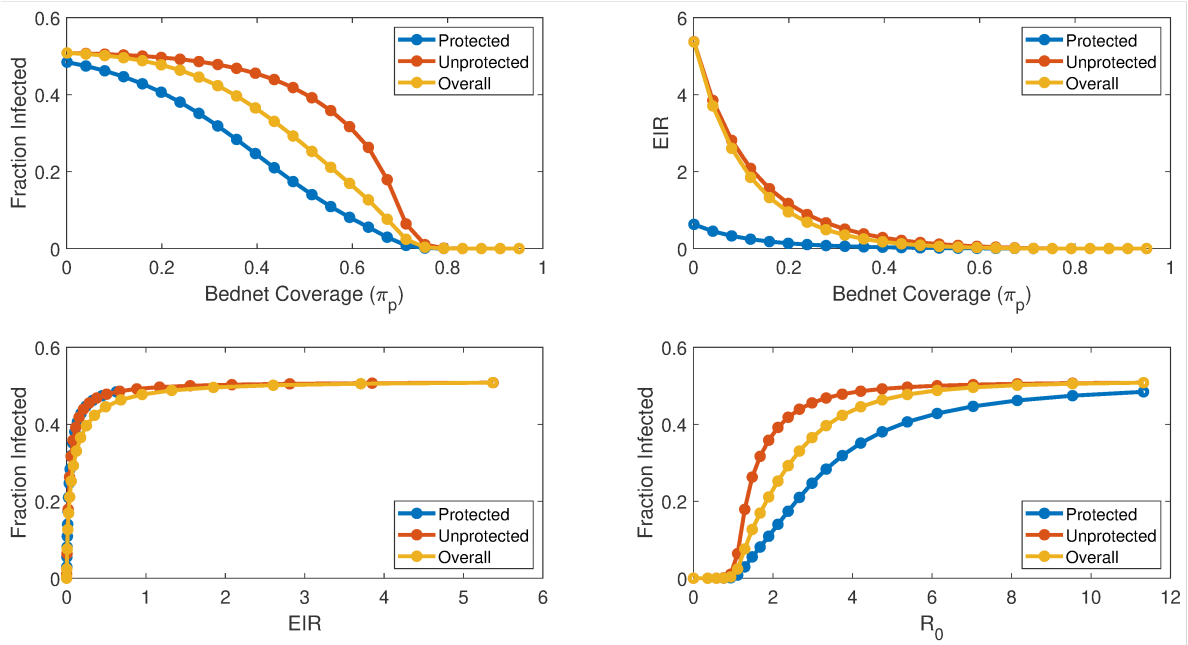

Figure 6: Relationships among EIR, fraction of infected humans, bednet coverage level, and $\tilde{\mathcal{R}}_0$, at the endemic equilibrium, as determined from numerical simulation of the model {(2.1), (2.2), (2.4)}, and for fixed temperature (25°C). Results are disaggregated between the protected, unprotected, and overall (bednet-protected and unprotected human) populations. Results are determined using baseline parameter values with a highly effective net in a holoendemic setting ($K_E = 100\frac{\Pi}{\mu_H}$, $\tilde{\mathcal{R}}_{0*} = 11.4$ with no bednet coverage).

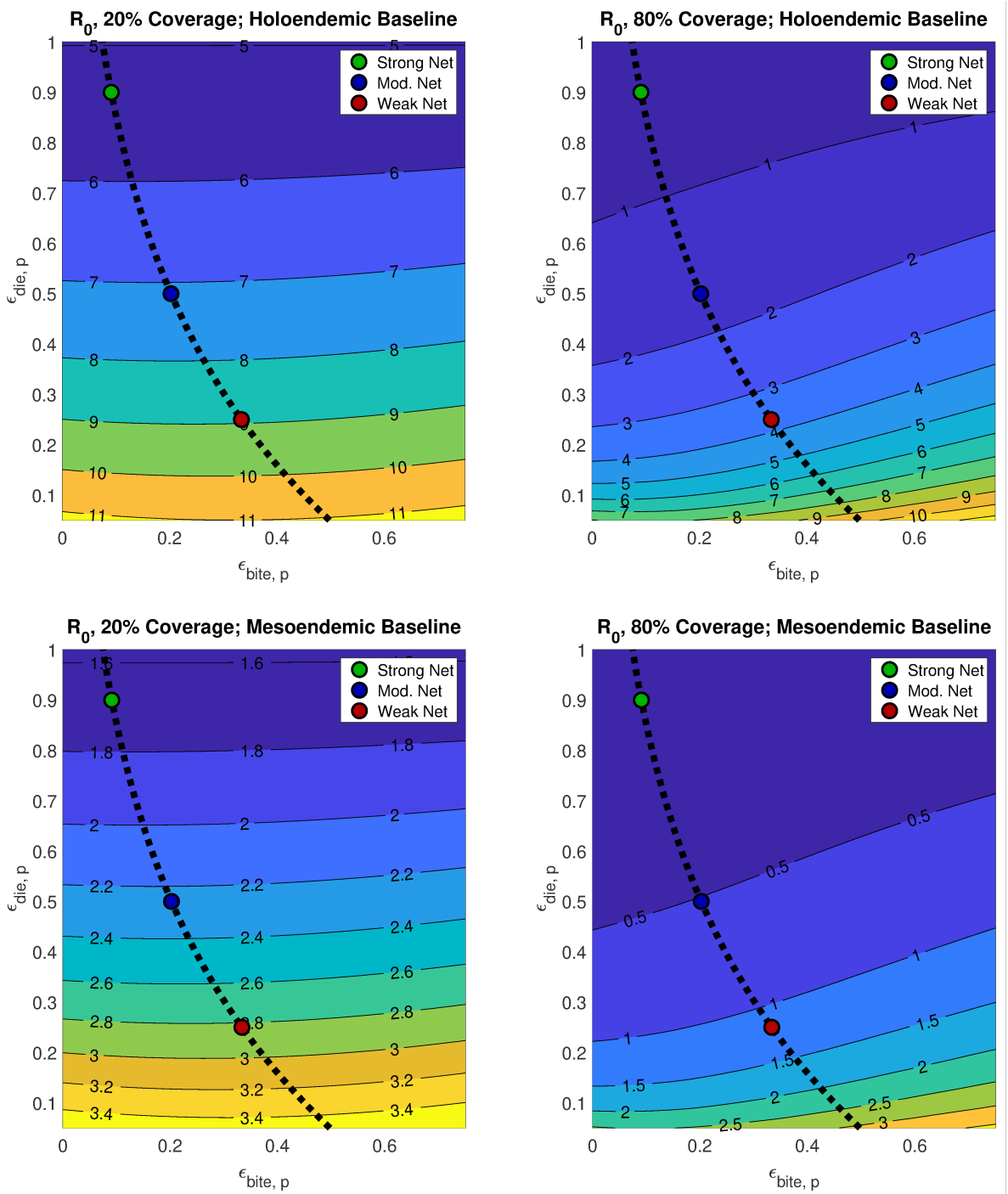

Figure 7: Contour plots of the $\tilde{\mathcal{R}}_0$ of the model {(2.1), (2.2), (2.4)}, as a function of $\varepsilon_{die,p}$ and $\varepsilon_{bite,p}$ (the respective probabilities that a mosquito dies or takes a blood meal upon encountering a protected human), for four different permutations of bednet coverage and baseline $\tilde{\mathcal{R}}_0$. The top panels use $K_E = 100\frac{\Pi}{\mu_H}$ to approximate a holoendemic baseline, while the bottom panels use $K_E = 10\frac{\Pi}{\mu_H}$ as an approximation of a mesoendemic baseline. Bednet coverage is either 20% (left) or 80% (right). The inscribed curve shows the approximate relationship between $\varepsilon_{die,p}$ and $\varepsilon_{bite,p}$ derived from experimental hut trial data (using the exponential relation given in Section 2.2), with three qualitative net effectiveness levels highlighted.

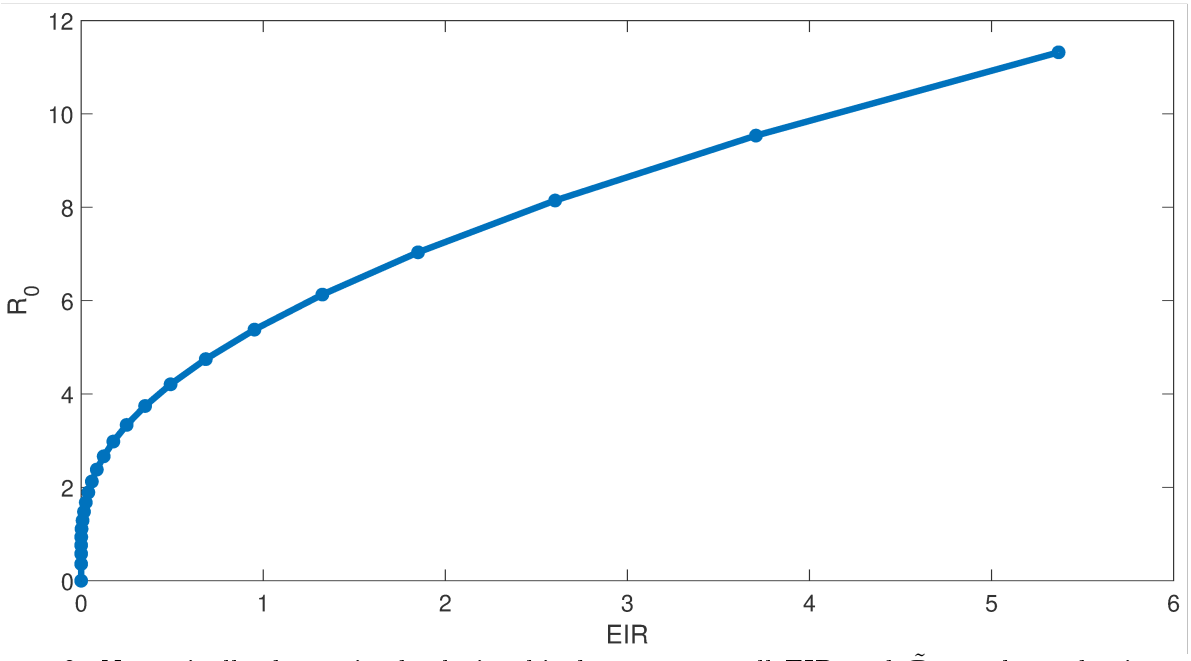

Figure 8: Numerically determined relationship between overall EIR and $\tilde{\mathcal{R}}_0$ at the endemic equilibrium, where variability in EIR is generated by changing bednet coverage, π_p. For larger EIR, $\tilde{\mathcal{R}}_0$ decreases nearly linearly with falling EIR, while for very small EIR, $\tilde{\mathcal{R}}_0$ decreases dramatically with falling EIR. Thus, EIR must be pushed very close to zero for malaria elimination. Results are generating using baseline parameter values with a highly effective net in a holoendemic setting ($K_E = 100\frac{\Pi}{\mu_H}$).

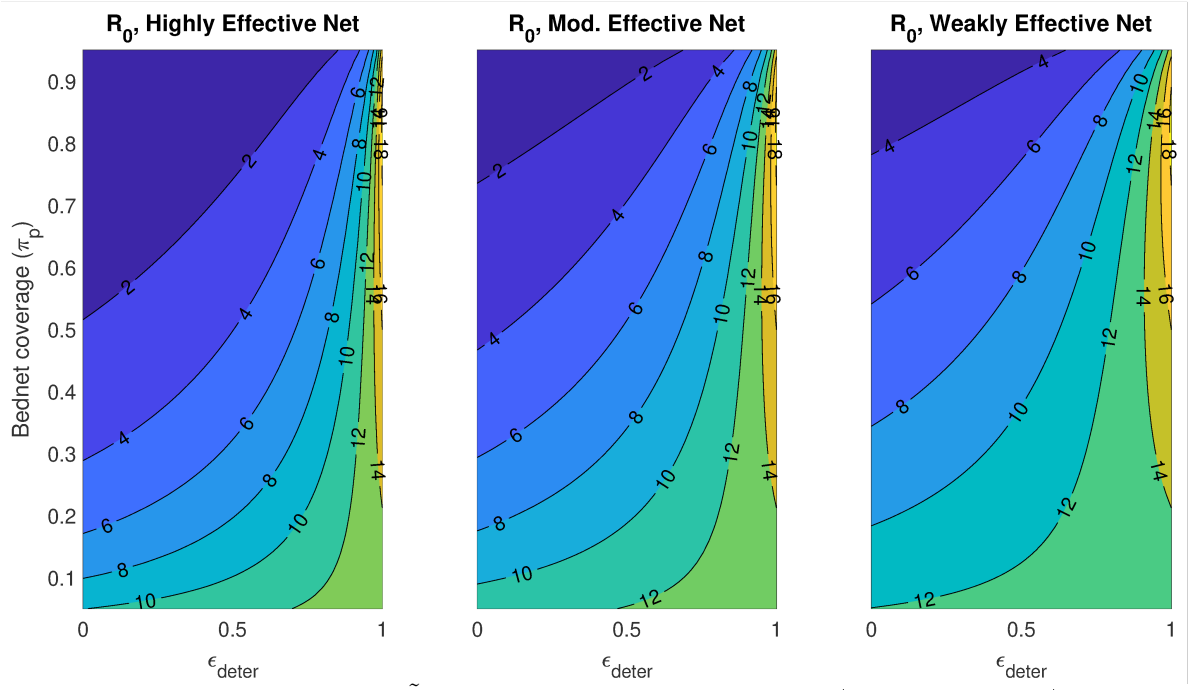

Figure 9: Contour plots showing $\tilde{\mathcal{R}}_0$ as a function of ε_{deter} and π_p (bednet coverage), for weakly, moderately, and highly effective nets. For this figure, we use $K_E = 100\frac{\Pi}{\mu_H}$ to approximate a holoendemic baseline.

4.2 Effects of Temperature

We examine the effect of changing mean ambient temperature (assumed equal to water temperature) upon $\tilde{\mathcal{R}}_0$ and EIR, as shown in Figure 10. We see an asymmetric increase in $\tilde{\mathcal{R}}_0$ and EIR from low temperatures to peaks around 29–30°C, followed by rapid drop-offs at higher temperatures. In other words, malaria burden is maximized for temperature values in the range 29–30°C, and such burden decreases for increasing temperatures thereafter. This peak is similar to that reported by Okuneye et al. [96], but higher than the reported value by the well-known Mordecai et al. [84] study. Furthermore, although the results in Figure 10 are obtained using a highly effective net with $K_E = 100 \times \Pi/\mu_H$, it should be stated that qualitatively similar results are obtained regardless of net type and K_E value.

To determine if temperature alters the qualitative interaction between bednet efficacy, bednet coverage, and control, we have generated a series of contour plots showing $\tilde{\mathcal{R}}_0$ as a function of $\varepsilon_{die,p}$ and $\varepsilon_{bite,p}$, for different ambient temperatures; several surfaces are given in Figure 11. While altering the maximum $\tilde{\mathcal{R}}_0$ value, changes in temperature have no meaningful effect upon the qualitative contour shape. That is, while maximum $\tilde{\mathcal{R}}_0$ varies between about 1.3 and 4.5 in the contours shown in Figure 11, the surface shapes are essentially invariant. Mirroring Figure 10, maximum $\tilde{\mathcal{R}}_0$ increases up to nearly 30°C and then falls off. Thus, it is concluded that bednet coverage and temperature independently affect malaria risk.

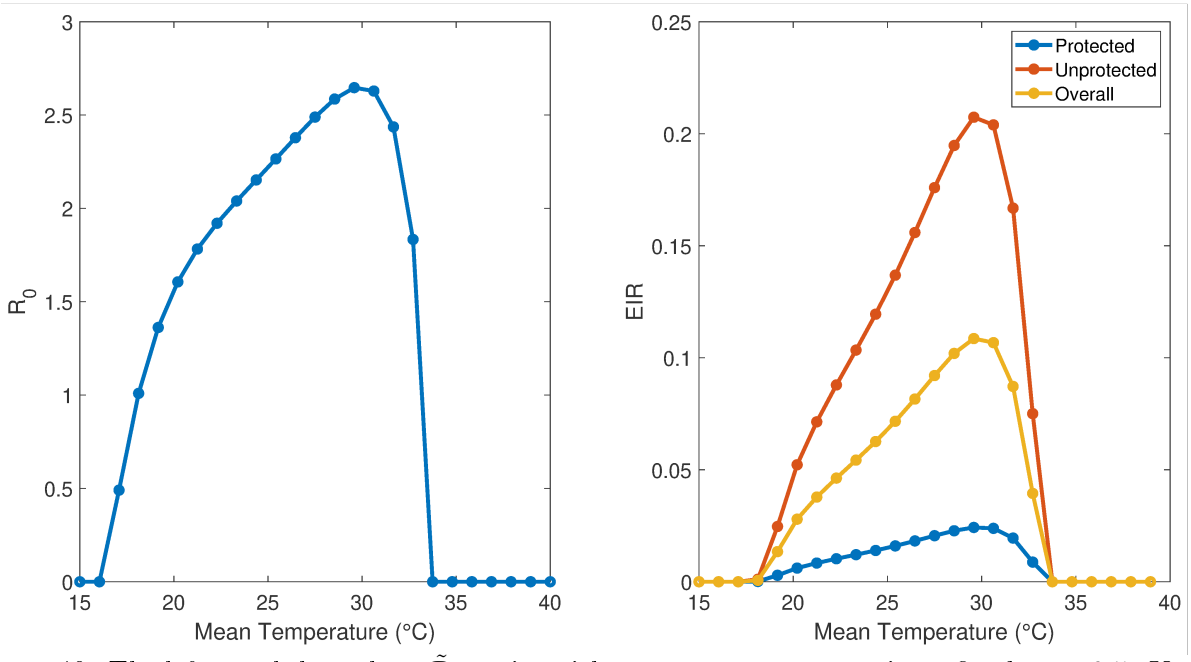

Figure 10: The left panel shows how $\tilde{\mathcal{R}}_0$ varies with mean temperature, using a fixed $\pi_p = 0.5$, $K_E = 100\frac{\Pi}{\mu_H}$, and a highly effective net. The right shows the numerically determined equilibrium values of EIR for protected, unprotected, and overall human populations as a function of temperature (and for the same parameter values). Both $\tilde{\mathcal{R}}_0$ and EIR, across populations, peak around 29°C.

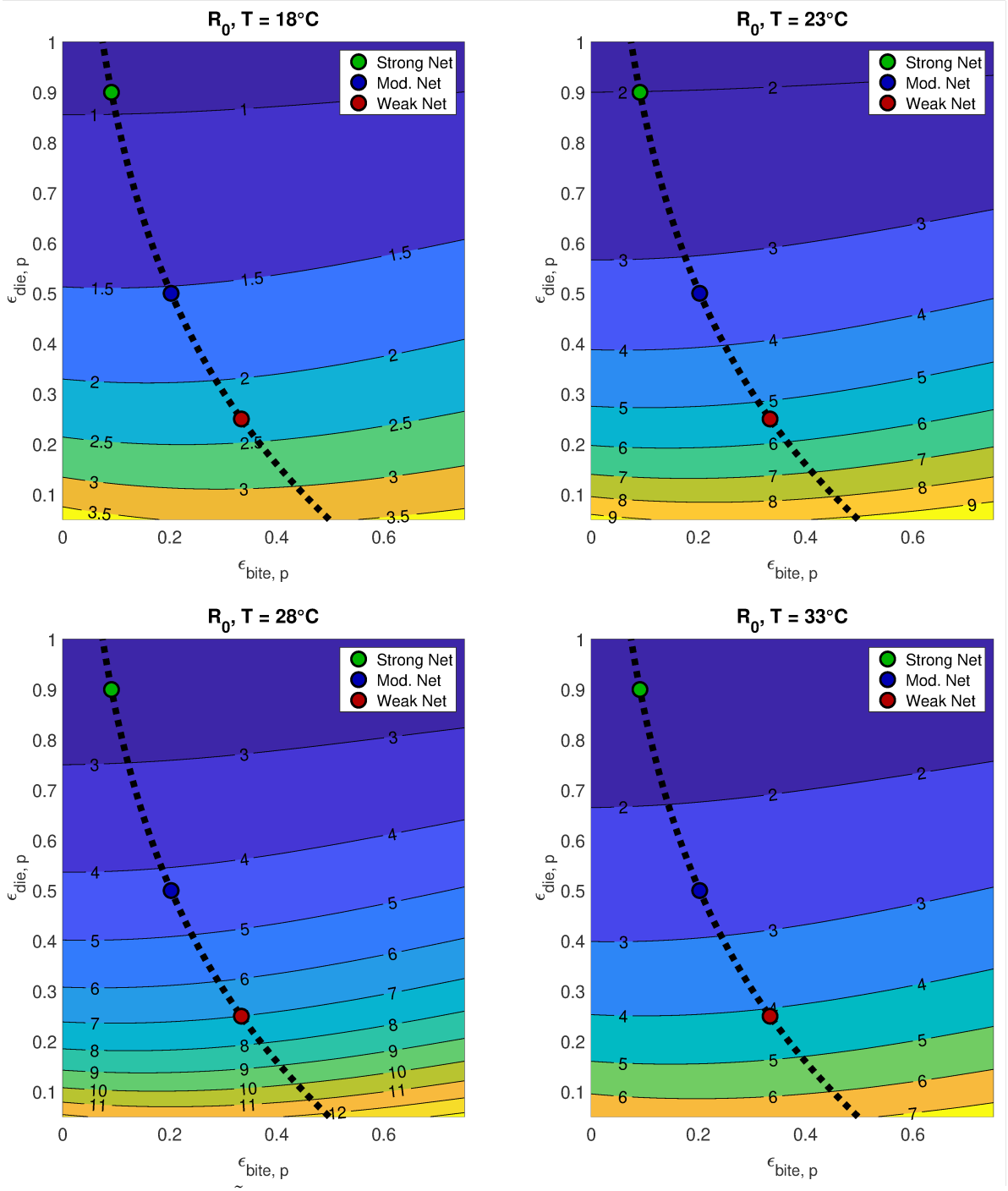

Figure 11: Contours of $\tilde{\mathcal{R}}_0$ as a function of $\varepsilon_{die,p}$ and $\varepsilon_{bite,p}$ for four different ambient temperatures, and for different net at 50% bednet coverage (with $K_E = 100\frac{\Pi}{\mu_H}$). The qualitative shape of the contour plots does not appreciably vary with temperature.

Discussion and Conclusions

Great success has been recorded in the concerted global effort against malaria over the past 15 years, thanks largely to the large-scale use of long-lasting insecticidal bednets (LLINs) and indoor residual spraying (IRS) in malaria-endemic regions within sub-Saharan Africa. There is now a strong global push to eradicate malaria (particularly the "Zero by 40" initiative of five chemical companies, with support of the Bill & Melinda Gates Foundation and the Innovative Vector Control Consortium [117, 119]). Given the widespread emergence of vector resistance to pyrethroid-based insecticides (the only chemical agent approved for use in LLINs), and the uncertainty surrounding how this affects (and will affect) malaria epidemiology, mathematical modeling studies are a promising to examine the interaction between bednet resistance and malaria epidemiology.

This paper presents a novel mathematical model, of the form of deterministic system of nonlinear differential equations, for gaining insight into the transmission dynamics of malaria in a population where a certain percentage of the populace use LLINs (consistently and correctly). In addition to incorporating many critical features of malaria disease (e.g., the four main cycles associated with malaria disease, namely immature mosquito life cycle, adult mosquito gonotrophic cycle, parasite sporogony in the mosquito and schizogony in humans; stratifying human population according to bednet usage; etc.), the model allows for the assessment of the killing and deterrence properties of the LLINs (in particular, in addition to killing adult mosquitoes (with some efficacy) upon encounter, the nets can also deter the mosquito from entering the house and/or from biting the human host). The model has been parametrized using ecological data and parameter values relevant to malaria transmission dynamics in holo- and meso-endemic regions of sub-Saharan Africa, and was used to evaluate the population-level impact of various LLINs coverage and effectiveness levels. For numerical simulation purposes, the effectiveness levels of the bednets described in Section 2.2 are considered.

The developed model was rigorously analysed to gain insight into its dynamical features (thereby allowing for the determination of important ecological and epidemiological thresholds that govern the persistence, effective control and/or elimination of the disease in a population). It is, first of all, shown, using the theory of center manifold [75], that the model undergoes the phenomenon of backward bifurcation, when the reproduction number of the model is less than 1, whenever a certain bifurcation coefficient attains positive values. This condition is associated with the disease-induced mortality in the host population being set to zero [60, 61]. The epidemiological implication of this phenomenon is that the usual epidemiological requirement of having the reproduction number of the model being less than 1, while necessary, is no longer sufficient for the effective control of the disease. Thus, when a backward bifurcation exists, greater control effort is needed to eradicate disease.

However, the phenomenon of backward bifurcation does not exist in the model developed in this study if all the values of the parameters are chosen from their biologically realistic ranges in Table 5, for a holoendemic setting, with five parameter values chosen outside the given range to illustrate a backward bifurcation. Thus, this study shows that, for a holoendemic malaria setting, the backward bifurcation phenomenon in the developed model is essentially a mathematical artifact which may not be realizable using realistic data (or set of parameter values). This result is consistent with those reported in [45, 46, 60, 61], which

also showed that backward bifurcation is not realizable using realistic parameters.

The backward bifurcation phenomenon is known to exist in vector-borne disease models that incorporate disease-induced death in the host(s) population(s). This is confirmed, in the current study, by showing that such bifurcation does not occur in the special case of the model with no disease-induced death in the human population (we showed, using Lyapunov function theory together with LaSalle's Invariance Principle, that the disease-free equilibrium of the special case of the model with no disease-induced death rate is, indeed, globally-asymptotically stable whenever the associated reproduction number is less than 1).

The impact of coverage level of the LLINs is monitored by simulating the model using various coverage levels. The simulation results obtained show, expectedly, that the disease prevalence in the host population (including those protected, by sleeping under a net, and the unprotected ones who do not sleep under a net) decreases with increasing coverage levels.

We observe LLINs at 20% coverage to reduce the reproduction number, at the holoendemic baseline (approximated by $K_E = 100 \times \Pi/\mu_H$), from a baseline value of about **11.7** to either **9.2, 7.3, or 5.5**, under weakly, moderately, or highly effective bednets, respectively. Increasing coverage to 80% yields $\tilde{\mathcal{R}}_0$ values of **3.6, 1.6, and 0.6**, for the same respective net efficacies. Thus, malaria elimination in holoendemic regions will require highly effective nets at high coverage levels. At the mesoendemic baseline, approximated by $K_E = 10 \times \Pi/\mu_H$ and giving $\tilde{\mathcal{R}}_0 =$ **3.7** without bednets, we see similar relative reductions in $\tilde{\mathcal{R}}_0$. However, given the lower baseline $\tilde{\mathcal{R}}_0$, even weakly effective nets give $\tilde{\mathcal{R}}_0 =$ **1.1** under 80% bednet coverage, near the elimination threshold, and both moderately and highly effective nets push $\tilde{\mathcal{R}}_0$ well below zero. Bednet coverage of 20%, in this case, improves malaria control, but is insufficient for elimination.

The widespread use of insecticide-based vector control interventions, including pyrethroid based insecticide-treated nets (ITNs; later replaced by long-lasting insecticidal nets (LLINs)) has resulted in the emergence of vector resistance to nearly every currently-available agent used in the insecticides [3, 38, 62, 126] with pyrethroid resistance now widely observed across the African continent [55]. Most nets distributed to-date are pyrethroid-only nets (although pyrethroid nets with the synergist PBO and pyrethroid nets with a second active ingredient are now available), and pyrethroid-only nets will likely remain a core vector control intervention over the next few years. As such it is critical to understand their current impact - now resistance to their active ingredients is so widespread - on malaria epidemiology. This study suggests that high coverage of weakly effective (i.e. low killing efficiency) nets is better than low coverage with highly effective (i.e. high killing efficiency) nets.

The impact of the deterrence property of LLINs to repel mosquitoes from entering protected house has also been examined, and we find, perhaps unexpectedly, that higher deterrence almost uniformly increases $\tilde{\mathcal{R}}_0$. This is likely because mosquitoes repelled from protected persons now focus their efforts on the unprotected subpopulation, thus increasing transmission within this group and potentially hampering elimination efforts.

The transmission cycle of malaria is greatly affected by changes in the environment. In particular, the life-cycles of the malaria vector (adult female *Anopheles* mosquito) and parasites (*Plasmodium*) are both strongly affected by changes in ambient temperature, while suitable aquatic habitat is necessary for immature mosquito development. Therefore, we

have examined how malaria burden changes with mean ambient temperature, and how this interacts with bednet coverage. We find $\tilde{\mathcal{R}}_0$ and EIR to both peak at just under 30°C, with this true regardless of bednet coverage levels. Indeed, we observe bednet coverage and temperature to essentially independently influence $\tilde{\mathcal{R}}_0$. Thus, somewhat colder regions, such as the eastern African highlands, may see an increase in malaria potential with climate change, while warmer western regions may be little affected.

Acknowledgements

One of the authors (ABG) is grateful to National Institute for Mathematical and Biological Synthesis (NIMBioS) for funding the Working Group on Climate Change and Vector-borne Diseases (VBDs). NIMBioS is an Institute sponsored by the National Science Foundation, the U.S. Department of Homeland Security, and the U.S. Department of Agriculture through NSF Award #EF-0832858, with additional support from The University of Tennessee, Knoxville. ABG also acknowledges the support, in part, of the Simons Foundation (Award #585022). We are very thankful to the two anonymous reviewers and the Handling Editor for their very insightful and constructive comments, which have significantly enhanced the manuscript.

References

[1] Agusto F.B., Gumel A.B. and Parham P.E. (2015). Qualitative assessment of the role of temperature variations on malaria transmission dynamics. *J. Biol. Syst.* **23**(4): 1-34.

[2] Alles, H. K., Mendis, K. N., and Carter, R. Malaria mortality rates in South Asia and in Africa: implications for malaria control (1998). *Parasitology Today.* **14**: 369 - 375.

[3] Alout H., Roche B., Dabiré R.K. and Cohuet A. 2017. Consequences of insecticide resistance on malaria transmission. *PLoS Pathog.* **13**(9):e1006499.

[4] Andrew H., Roberto G., Kyros K., Alekos S., Carla S., Dimitris K., Matthew G., Dean B., Eric M., Steven R., Austin B., Nikolai W., Andrea C. and Tony N. (2015). A CRISPR-Cas9 gene drive system targeting female reproduction in the malaria mosquito vector *Anopheles gambiae*. *Nature Biotechnology.* doi:10.1038/nbt.3439.

[5] Aron J.L and May R. The population dynamics of malaria. Population dynamics and infectious disease London: Chapman and Hall. 1982; p. 139-179.

[6] Asale A., Getachew Y., Hailesilassie W., Speybroeck N., Duchateau L. and Yewhalaw D. (2014). Evaluation of the efficacy of DDT indoor residual spraying and long-lasting insecticidal nets against insecticide resistant populations of *Anopheles arabiensis Patton (Diptera: Culicidae)* from Ethiopia using experimental huts. *Parasites and vectors.* **7**(1), 131.

[7] Asidi A.N., N'Guessan, R., Hutchinson R.A., Traorá Lamizana M., Carnevale P. and Curtis C.F. (2004). Experimental hut comparisons of nets treated with carbamate or pyrethroid insecticides, washed or unwashed, against pyrethroid-resistant mosquitoes. *Medical and veterinary entomology.* **18**(2), 134-140.

[8] Asidi A.N., N'Guessan R., Koffi A.A., Curtis C.F., Hougard J.M., Chandre F. and Rowland M.W. (2005). Experimental hut evaluation of bednets treated with an organophosphate (chlorpyrifos-methyl) or a pyrethroid (lambdacyhalothrin) alone and in combination against insecticide-resistant *Anopheles gambiae* and *Culex quinquefasciatus* mosquitoes. *Malaria journal.* **4**(1), 25.

[9] Ashley, E. A., and White, N. J. The duration of *Plasmodium falciparum* infections (2014). *Malaria Journal.* **13**: 500.

[10] Barbosa S, Hastings IM. (2012). The importance of modeling the spread of insecticide resistance in a heterogeneous environment: the example of adding synergists to bednets. *Malaria Journal.* **11:**258.

[11] Bayili K., N'do S., Namountougou M., Sanou R., Ouattara A., Dabiré R. K., and Diabaté A. (2017). Evaluation of efficacy of Interceptor® G2, a long-lasting insecticide net coated with a mixture of chlorfenapyr and alpha-cypermethrin, against pyrethroid resistant *Anopheles gambiae sl* in Burkina Faso. *Malaria journal.* **16**(1), 190.

[12] Bayoh, M.N. Studies on the development and survival of *Anopheles gambiae sensu stricto* at various temperatures and relative humidities. Doctoral dissertation. Durham Theses, Durham University. (2001). http://etheses.dur.ac.uk/4952/.

[13] Bayoh, M.N., and Lindsay, S.W. Effect of temperature on the development of the aquatic stages of *Anopheles gambiae sensu stricto (Diptera: Culicidae)* (2003). *Bulletin of Entomological Research.* 93: 375 - 381.

[14] Bayoh, M. N., and Lindsay, S. W. Temperature-related duration of aquatic stages of the Afrotropical malaria vector mosquito Anopheles gambiae in the laboratory (2004). *Medicaland Veterinary Entomology.* **18**: 174 - 179.

[15] Beck-Johnson LM, Nelson WA, Paaijmans KP, Read AF, Thomas MB, BjØrnstad ON. 2017. The importance of temperature fluctuations in understanding mosquito population dynamics and malaria risk. *R. Soc. Open Sci.* **4:** 160969. http://dx.doi.org/10.1098/rsos.160969.

[16] Bhatt S, Weiss DJ, Cameron E, Bisanzio D, Mappin B, Dalrymple U, Battle K, Moyes CL, Henry A, Eckhoff PA, Wenger EA, Briët O, Penny MA, Smith TA, Bennett A, Yukich J, Eisele TP, Griffin JT, Fergus CA, Lynch M, Lindgren F, Cohen JM, Murray CLJ, Smith DL, Hay SI, Cibulskis RE, Gething PW. 2015. The effect of malaria control on Plasmodium falciparum in Africa between 2000 and 2015. *Nature.* **526:**207-211.

[17] Birget PLG, Koella JC. 2015. A genetic model of the effects of insecticide-treated bed nets on the evolution of insecticide-resistance. *Evolution, Medicine, and Public Health* 205-215.

[18] P.L.G. Birget and J.C. Koella (2015). An Epidemiological model of the effects of insecticide treated bed nets on malaria transmission. *PLoS ONE* 10(12): e0144173. doi:10.1371/journal. pone.0144173.

[19] Blayneh K., Gumel A.B., Lenhart S. and Clayton T. (2010). Backward bifurcation analysis and optimal control of West Nile virus. *Bull. Math. Biol.* **72**(4): 1006-1028.

[20] Briere J.F., Pracros P., le Roux A.Y. and Pierre S. (1999). A novel rate model of temperature-dependent development for arthropods. *Environmental Entomology*, **28**, 22-29.

[21] Brown Z.S., Dickinson K.L. and Kramer R.A. (2013). Insecticide resistance and malaria vector control: the importance of fitness cost mechanisms in determining economically optimal control trajectories. *Journal of Economic Entomology.* **106**(1): 366-374.

[22] Camara S., Alou L.P.A., Koffi A.A., Clegban Y.C.M., Kabran J.P., Koffi F.M. and Pennetier C. (2018). Efficacy of Interceptor® G2, a new long-lasting insecticidal net against wild pyrethroid-resistant Anopheles gambiae ss from Côte d'Ivoire: a semi-field trial. *Parasite*, 25, 42.

[23] Carr J., Application of Centre Manifold Theory, *Springer-Verlag, New York*, 1981.

[24] Castillo-Chavez C.C. and Song B., Dynamical models of tuberculosis and their applications (2004). *Math. Biosci. Engrg.* 1 361-404.

[25] Charlwood, J. D., Smith, T., Billingsley, P. F., Takken, W., Lyimo, E. O. K., and Meuwissen, J. H. E. T. Survival and infection probabilities of anthropophagic anophelines from an area of high prevalence of *Plasmodium falciparum* in humans (1997). *Bulletin of Entomological Research.* **87**: 445 - 453.

[26] Cheeseman I.H., Miller B.A., Nair S., Nkhoma S., Tan A., Tan J.C., Al-Saai S., Phyo A.P., Moo C.L., Lwin K.M., McGready R., Ashley E., Imwong M., Stepniewska K., Yi P., Dondorp A.M., Mayxay M., Newton P.N., White N.J., Nosten F., Ferdig M.T. and Anderson T.J. (2012). A major genome region underlying artemisinin resistance in malaria. *Science* 79-82. DOI:10.1126/science.1215966.

[27] Chandre F., Darriet F., Duchon S., Finot L., Manguin S., Carnevale, P. and Guillet P. (2000). Modifications of pyrethroid effects associated with kdr mutation in *Anopheles gambiae*. *Medical and veterinary entomology.* **14**(1), 81-88.

[28] Chitnis N., Smith T. and Steketee R. (2009). A mathematical model for the dynamics of malaria in mosquitoes feeding on a heterogeneous host population. *Journal of Biological Dynamics*, 2:3, 259-285.

[29] Churcher T.S., Lissenden N., Griffin J.T., Worrall E. and Ranson H. (2016). The impact of pyrethroid resistance on the efficacy and effectiveness of bednets for malaria control in Africa. *eLife* 5:e16090. DOI: 10.7554/eLife.16090.

[30] David *et al.* Predicting changing malaria risk after expanded insecticide-treated net coverage in Africa. *Trends in Parasitology* Vol.25 No.11.

[31] Cator, L. J., Lynch, P. A., Read, A. F., & Thomas, M. B. (2012). Do malaria parasites manipulate mosquitoes?. *Trends in parasitology.* **28**(11), 466-470.

[32] Corbel V., Chandre F., Brengues C., Akogbéto M., Lardeux F., Hougard J. M. and Guillet, P. (2004). Dosage-dependent effects of permethrin-treated nets on the behaviour of *Anopheles gambiae* and the selection of pyrethroid resistance. *Malaria Journal.* **3**(1), 22.

[33] Corbel V., Chabi J., Dabiré R. K., Etang J., Nwane P., Pigeon O. and Hougard J.M. (2010). Field efficacy of a new mosaic long-lasting mosquito net (PermaNet® 3.0) against pyrethroid-resistant malaria vectors: a multi centre study in Western and Central Africa. *Malaria Journal.* **9**(1), 113.

[34] Detinova, T. S., Bertram, D. S., and World Health Organization. Age grouping methods in Diptera of medical importance with special reference to some vectors of malaria (1962).

[35] Djènontin A., Alou L. P. A., Koffi A., Zogo B., Duarte E., N'Guessan R. and Pennetier, C. (2015). Insecticidal and sterilizing effect of Olyset Duo®, a permethrin and pyriproxyfen mixture net against pyrethroid-susceptible and-resistant strains of *Anopheles gambiae ss*: a release-recapture assay in experimental huts. *Parasite*, 22, 27.

[36] Djènontin A., Moiroux N., Bouraïma A., Zogo B., Sidick I., Corbel V. and Pennetier, C. (2018). Field efficacy of a new deltamethrin long lasting insecticidal net (LifeNet®) against wild pyrethroid-resistant Anopheles gambiae in Benin. *BMC public health.* **18**(1), 947.

[37] Dondorp, A. M., Fanello, C. I., Hendriksen, I. C., Gomes, E., Seni, A., Chhaganlal, K.D., and Kivaya, E. Artesunate versus quinine in the treatment of severe falciparum malaria in African children (AQUAMAT): an open-label, randomised trial (2010). *The Lancet.* **376**: 1647 - 1657.

[38] Dondorp A.M., Nosten F, Yi P, Das D, Phyo AP, Tarning J. and White NJ. 2009. Artemisinin resistance in *Plasmodium falciparum* malaria. *New England Journal of Medicine.* **361**(5):455-467.

[39] Dumont Y. and Chiroleu F. (2010). Vector control for the chikungunya disease. *Math. Biosci. Engrg.* **7**: 105-111.

[40] Eikenberry S. E. and Gumel A.B. (2018) Mathematical modeling of climate change and malaria transmission dynamics: a historical review. *J. Math. Biol.* **77**:857-933.

[41] Eikenberry S. E. and Gumel A.B: Nonlinear relationship between bednet insecticide resistance and malaria entomologic inoculation rate: Results from a data-driven mathematical model. Under preparation.

[42] Fanello C., Kolaczinski J. H., Conway D.J., Carnevale P. and Curtis, C. F. (1999). The kdr pyrethroid resistance gene in *Anopheles gambiae*: tests of non-pyrethroid insecticides and a new detection method for the gene. *Parassitologia.* **41**(1-3), 323-326.

[43] Feng X., Ruan S., Teng Z. and Wang K. (2015). Stability and backward bifurcation in a malaria transmission model with applications to the control of malaria in China . *Mathematical Biosciences.* **266**: 52-64.

[44] Filipe, J. A., Riley, E. M., Drakeley, C. J., Sutherland, C. J., and Ghani, A. C. (2007). Determination of the processes driving the acquisition of immunity to malaria using a mathematical transmission model. *PLoS Computational Biology.* 3: e255.

[45] Garba S.M., Gumel A.B. and Abu Bakar M.R. (2008). Backward bifurcations in dengue transmission dynamics. *Mathematical Biosciences.* **215**(1): 11-25.

[46] Garba S.M. and Gumel A.B. (2010). Effect of cross-immunity on the transmission dynamics of two strains of dengue. *Int. J. of Math.* **87**(10): 2361-2384.

[47] Gamboa D, Ho MF, Bendezu J, Torres K, Chiodini PL, Barnwell JW, and Cheng Q. (2010). A large proportion of *P. falciparum* isolates in the Amazon region of Peru lack *pfhrp2* and *pfhrp3*: Implications for malaria rapid diagnostic tests. PLoS ONE. **5(1):**e8091. https://doi.org/10.1371/journal.pone.0008091.

[48] Gates, B. We can eradicate malaria within a generation. https://www.gatesnotes.com/Malaria (accessed January 2016).

[49] Gething P.W., Smith D.L., Patil A.P., Tatem A.J., Snow R.W. and Hay S.I. (2010). Climate change and the global malaria recession. *Nature.* **465**:342-345.

[50] Gething P.W., Patil A.P., Smith D.L., Guerra C.A., Elyazar I.R., Johnston G.L., Tatem A.J., Ha S.I. (2011). A new world malaria map: *Plasmodium falciparum* endemicity in 2010. *Malaria J* **10:** 378.

[51] Gething P.W., Casey D.C., Weiss D.J. et al., and Kutz M.J. (2016). Mapping *Plasmodium falciparum* mortality in Africa between 1990 and 2015. *New England Journal of Medicine* **375(25):**2435-2445.

[52] Githeko A.K., Brandling-Bennett A.D., Beier M., Atieli F., Owaga M. and Collins F.H. (1992). The reservoir of *Plasmodium falciparum* malaria in a holoendemic area of western Kenya. *Transactions of The Royal Society of Tropical Medicine and Hygiene* **86**(4): 355-358

[53] Glunt KD, Coetzee M, Huijben S, Koffi AA, Lynch PA, N'Guessan R, Oumbouke WA, Sternberg ED, Thomas MB. (2018). Empirical and theoretical investigation into the potential impacts of insecticide resistance on the effectiveness of insecticide-treated bed nets. Evolutionary applications. 11(4):431-441.

[54] Hawley W.A., Kuile FO, Steketee RS, Nahlen BL et al. (2003). Implications of the western Kenya permethrin-treated bed net study for policy, program implementation, and future research. *Am. J. Tropical Med. Hygiene.* **68** (Suppl. 4): 168-173.

[55] Hemingway J., Ranson H., Magill A., Kolaczinski J., Fornadel C., Gimnig J., Coetzee M., Simard F., Roch D.K., Hinzoumbe C.K., Pickett J. (2016). Averting a malaria disaster: will insecticide resistance derail malaria control?. *The Lancet.* **387**(10029):1785-8.

[56] Hien, A.S., Soma, D.D., Hema, O., Bayili, B., Namountougou, M., Gnankiné, O., Dabiré, K. R. (2017). Evidence that agricultural use of pesticides selects pyrethroid resistance within *Anopheles gambiae s.l.* populations from cotton growing areas in Burkina Faso, West Africa. *PLoS ONE*, 12(3), e0173098. https://doi.org/10.1371/journal.pone.0173098

[57] Himeidan Y.E., Kweka E.J. (2012). Malaria in the East African highlands during the past 30 years: impact of environmental changes. *Frontiers of Physiology.* **3**(315):1-11.

[58] Holzer B.R., Egger M., Teuscher T., Koch S., Mboya D.M., Smith G.D.(1993) Childhood anemia in Africa: to transfuse or not transfuse? *Acta Trop.* 55(1-2):47-51.

[59] Huijben S. and Paaijmans K.P. (2017). Putting evolution in elimination: Winning our ongoing battle with evolving malaria mosquitoes and parasites. *Evolutionary Applications.* **11**(4):415-430.

[60] Iboi E.A. and Gumel A.B. (2018). Mathematical assessment of the roles of temperature and *Dengvaxia* vaccine on the transmission dynamics of dengue serotypes. *Mathematical Biosciences.* **304**: 25-47.

[61] Iboi E., Okuneye K., Sharomi O. and Gumel A. B. (2018). Comments on "A Mathematical study to control visceral leishmaniasis: An application to South Sudan" *Bull Math Biol.* **80**: 825-839.

[62] Imwong M, Suwannasin K, Kunasol C, Sutawong K, Mayxay M, Rekol H, ⋯ Dondorp AM. 2017. The spread of artemisinin-resistant *Plasmodium falciparum* in the Greater Mekong Subregion: a molecular epidemiology observational study. The Lancet Infectious Diseases. https://doi.org/10.1016/S1473-3099(17)30048-8.

[63] Jeffery, G. M. and Eyles, D. E. The duration in the human host of infections with a Panama strain of *Plasmodium falciparum* (1954). *The American Journal of Tropical Medicine and Hygiene.* **3**: 219 - 224.

[64] Johnston GL, Smith DL, Fidock DA. 2013. Malaria's missing number: calculating the human component of $\mathcal{R}_0$ by a within-host mechanistic model of *Plasmodium falciparum* infection and transmission. *PLoS Comput Biol* **9**(4): e1003025. doi:10.1371/journal.pcbi.1003025

[65] Kabula B, Kisinza W, Tungu P, Ndege C, Batengana B, Kollo D, Malima R, Kafuko J, Mohamed M, Magesa S. 2014. Co-occurrence and distribution of East (L1014S) and West (L1014F) African knock down resistance in *Anopheles gambiae sensu lato* population of Tanzania. *Trop. Med. Int. Health.* **19**(3): 331-41.

[66] Ketoh G.K., Ahadji-Dabla K.M., Chabi J., Amoudji A.D., Apetogbo G.Y., Awokou F. and Glitho, I.A. (2018). Efficacy of two PBO long lasting insecticidal nets against natural populations of *Anopheles gambiae sl* in experimental huts, Kolokopé, Togo. *PloS one.* **13**(7), e0192492.

[67] Killeen GF, Smith TA. (2007). Exploring the contributions of bed nets, cattle, insecticides and excitorepellency to malaria control: a deterministic model of mosquito host-seeking behaviour and mortality. Transactions of the Royal Society of Tropical Medicine and Hygiene. 101(9):867–80.

[68] Killeen GF, Chitnis N, Moore SJ, Okumu FO. (2011). Target product profile choices for intra-domiciliary malaria vector control pesticide products: repel or kill?. Malaria journal. 10(1):207.

[69] Kleinschmidt I., Bradley J., Knox T., Mnzava A.P., Kafy H. *et al.* (2018). Implications of insecticide resistance for malaria vector control with longlasting insecticidal nets: a WHO-coordinated, prospective, international, observational cohort study. *The Lancet Infectious Diseases.* **18**(6) 640-649.

[70] Koffi A.A., Alou L.P.A., Djenontin A., Kabran J.P.K., Dosso Y., Kone A. and Pennetier C. (2015). Efficacy of Olyset® Duo, a permethrin and pyriproxyfen mixture net against wild pyrethroid-resistant *Anopheles gambiae ss* from Côte d'Ivoire: an experimental hut trial. *Parasite.* 22, 28.

[71] Kozycki C.T., Umulisa N., Rulisa S., Mwikarago E.I., Musabyimana J.P., Habimana J.P. and Krogstad DJ. 2017. False-negative malaria rapid diagnostic tests in Rwanda: impact of *Plasmodium falciparum* isolates lacking *hrp2* and declining malaria transmission. *Malaria Journal.* **16:**123. https://doi.org/10.1186/s12936-017-1768-1.

[72] Kweka E.J., Lyaruu L.J. and Mahande A.M. (2017). Efficacy of PermaNet® 3.0 and PermaNet® 2.0 nets against laboratory-reared and wild *Anopheles gambiae sensu lato* populations in northern Tanzania. *Infectious diseases of poverty.* **6**(1), 11.

[73] Lines, J.D., Wilkes, T. J., and Lyimo, E. O.(1991). Human malaria infectiousness measured by age-specific sporozoite rates in *Anopheles gambiae* in Tanzania. *Parasitology.* **102**:167 - 177.

[74] Lakshmikantham V., Leela S., and Martynyuk A. A., Stability Analysis of Nonlinear Systems, Marcel Dekker, New York, NY, USA, 1989.

[75] LaSalle J. and Lefschetz S. The Stability of Dynamical Systems, SIAM, Philadelphia, 1976.

[76] Levitz L., Janko M., Mwandagalirwa K., Thwai K.L., Likwela J.L., Tshefu A.K., Emch M. and Meshnick S.R. (2018). Effect of individual and community-level bed net usage on malaria prevalence among under-fives in the Democratic Republic of Congo. *Malar J.* **17**(1):39.

[77] Macdonald G. 1957. The Epidemiology and Control of Malaria. Oxford University Press.

[78] Mathenge E.M, Gimnig J.E, Kolczak M, Ombok M, Irungu L.W, Hawley W.A. (2001). Effect of permethrin-impregnated nets on exiting behavior, blood feeding success, and time of feeding of malaria mosquitoes *(Diptera: Culicidae)* in western Kenya. *Journal of Medical Entomology.* **38**(4):531-536. Available from:http://www.bioone.org/doi/abs/10.1603/0022-2585-38.4.531 doi 10.1603/0022-2585-38.4.531 PMID:11476333.

[79] Le Menach A, Takala S, McKenzie FE, Perisse A, Harris A, Flahault A, Smith DL. (2007). An elaborated feeding cycle model for reductions in vectorial capacity of night-biting mosquitoes by insecticide-treated nets. Malaria journal. 6(1):10.

[80] Malima R.C., Magesa S.M., Tungu P.K., Mwingira V., Magogo F. S., Sudi W. and Rowland M. (2008). An experimental hut evaluation of Olyset® nets against *anopheline* mosquitoes after seven years use in Tanzanian villages. *Malaria journal.* **7**(1), 38.

[81] Malima R., Tungu P.K., Mwingira V., Maxwell C., Magesa S.M., Kaur H. and Rowland M. (2013). Evaluation of the long-lasting insecticidal net Interceptor LN: laboratory and experimental hut studies against *anopheline* and *culicine* mosquitoes in northeastern Tanzania. *Parasites and vectors.* **6**(1), 296.

[82] Mohammed-Awel J. and Numfor E. (2017). Optimal insecticide treated bednet coverage and malaria treatment in a Malaria-HIV co-infection model. *Journal of Biological Dynamics.* **11:**160-191.

[83] Mohammed-Awel J., Agusto F., Mickens R.E. and Gumel A.B. (2018). Mathematical assessment of the role of vector insecticide resistance and feeding/resting behavior on malaria transmission dynamics: optimal control analysis. *Infectious Disease Modelling.* **3**: 301-321.

[84] Mordecai, E.A., Paaijmans K.P., Johnson L.R., Balzer C., Ben-Horin T., de Moor E., McNally A., Pawar S., Ryan S.J., Smith T.C. and Lafferty K.D. (2013). Optimal temperature for malaria transmission is dramatically lower than previously predicted. *Ecology Letters.* **16**: 22-30.

[85] D. Moulay, M.A. Aziz-Alaoui and M. Cadivel .The chikungunya disease: Modeling, vector and transmission global dynamics (2011). *Math. Biosci.* **229**: 50-63.

[86] Mutuku F.M., King C.H., Mungai P., Mbogo C., Mwangangi J., Muchiri E.M., Walker E.D. and Kitron U (2011). Impact of insecticide-treated bed nets on malaria transmission indices on the south coast of Kenya.*Malaria Journal.* **10**:356

[87] Nájera JA, González-Silva M, Alonso PL. 2011. Some lessons for the future from the Global Malaria Eradication Programme (1955-1969). *PLoS Med* **8**(1):e1000412.

[88] Ngonghala, C. N., Ngwa, G. A., and Teboh-Ewungkem, M. I (2012). Periodic oscillations and backward bifurcation in a model for the dynamics of malaria transmission. *Mathematical Biosciences.* **240**(1): 45 -62.

[89] N'Guessan R., Darriet F., Doannio J.M.C., Chandre F. and Carnevale P. (2001). Olyset Net® efficacy against pyrethroid-resistant *Anopheles gambiae* and *Culex quinquefasciatus* after 3 years field use in Côte d'Ivoire. *Medical and veterinary entomology.* **15**(1), 97-104.

[90] N'Guessan R., Corbel V., Akogbéto M. and Rowland M. (2007). Reduced efficacy of insecticide-treated nets and indoor residual spraying for malaria control in pyrethroid resistance area, Benin. *Emerging infectious diseases* **13**(2), 199-206.

[91] N'Guessan R., Asidi A., Boko P., Odjo A., Akogbeto M., Pigeon O. and Rowland M. (2010). An experimental hut evaluation of PermaNet® 3.0, a deltamethrin-piperonyl butoxide combination net, against pyrethroid-resistant *Anopheles gambiae* and *Culex quinquefasciatus* mosquitoes in southern Benin. *Transactions of the Royal Society of Tropical Medicine and Hygiene.* **104**(12), 758-765.

[92] Ngufor C., N'Guessan R., Fagbohoun J., Odjo A., Malone D., Akogbeto M. and Rowland M. (2014). Olyset Duo® (a pyriproxyfen and permethrin mixture net): an experimental hut trial against pyrethroid resistant *Anopheles gambiae* and *Culex quinquefasciatus* in Southern Benin. *PLoS One.* **9**(4), e93603.

[93] Ngufor C., N'Guessan R., Boko P., Odjo A., Vigninou E., Asidi A. and Rowland M. (2011). Combining indoor residual spraying with chlorfenapyr and long-lasting insecticidal bed nets for improved control of pyrethroid-resistant *Anopheles gambiae*: an experimental hut trial in Benin. *Malaria journal.* **10**(1), 343.

[94] Ngufor C., N'guessan R., Fagbohoun J., Todjinou D., Odjo A., Malone D. and Rowland M. (2016). Efficacy of the Olyset Duo net against insecticide-resistant mosquito vectors of malaria. *Science translational medicine.* **8**(356), 356ra121-356ra121.

[95] Okumu F.O. and Moore S.J. (2011). Combining indoor residual spraying and insecticide-treated bednets for malaria control in Africa: a review of possible outcomes and an outline of suggestions for the future. *Malaria Journal.* **10:**208.

[96] Okuneye K., Eikenberry S.E., and Gumel A.B. (2019). Weather-driven Malaria Transmission Model with Gonotrophic and Sporogonic Cycles (2019). *Journal of Biological Dynamics.* **13**(1): 288-324.

[97] Okumu F.O., Kiware S.S., Moore S.J. and Killeen G.F. (2013). Mathematical evaluation of community level impact of combining bed nets and indoor residual spraying upon malaria transmission in areas where the main vectors are Anopheles arabiensis mosquitoes. Parasites & vectors. 6(1):17.

[98] Paaijmans, K.P., Blanford, S., Bell, A.S., Blanford, J.I., Read, A.F., and Thomas M. B. Influence of climate on malaria transmission depends on daily temperature variation (2010). *Proceedings of the National Academy of Sciences.* **107**: 15135-15139.

[99] Oxborough R.M., Kitau J., Matowo J., Feston E., Mndeme R., Mosha F.W. and Rowland M.W. (2013). ITN mixtures of chlorfenapyr (pyrrole) and alphacypermethrin (pyrethroid) for control of pyrethroid resistant *Anopheles arabiensis* and *Culex quinquefasciatus*. *PLoS One.* **8**(2), e55781.

[100] Pennetier C., Bouraima A., Chandre F., Piameu M., Etang J., Rossignol M., ... and Pigeon O. (2013). Efficacy of Olyset® Plus, a new long-lasting insecticidal net incorporating permethrin and piperonil-butoxide against multi-resistant malaria vectors. *PLoS One.* **8**(10), e75134.

[101] Phyo A.P., Nkhoma S., Stepniewska K., Ashley E.A., Nair S., McGready R., ler Moo C., Al-Saai S., Dondorp A.M., Lwin K.M., Singhasivanon P., Day N.P., White N.J., Anderson T.J. and Nosten F. (2012). Emergence of artemisinin-resistant malaria on the western border of Thailand: a longitudinal study. *Lancet* 1-7. DOI:10.1016/S0140-6736(12)60484-X

[102] N. Protopopoff J.F., Mosha E., Lukole J.D., Charlwood A. Wright C.D., Mwalimu A., Manjurano F.W., Mosha W., Kisinza I., Kleinschmidt and Rowland M. (2018). Effectiveness of a long-lasting piperonyl butoxide-treated insecticidal net and indoor residual spray interventions, separately and together, against malaria transmitted by pyrethroid-resistant mosquitoes: a cluster, randomised controlled, two-by-two factorial design trial. *The Lancet.* **391**(10130): 1577-1588.

[103] Randriamaherijaona S., Briët O.J., Boyer S., Bouraima A., N'Guessan R., Rogier C. and Corbel V. (2015). Do holes in long-lasting insecticidal nets compromise their efficacy against pyrethroid resistant *Anopheles gambiae* and *Culex quinquefasciatus*? Results from a release-recapture study in experimental huts. *Malaria journal.* **14**(1), 332.

[104] Reid, M.C. and McKenzie, F.E. (2016). The contribution of agricultural insecticide use to increasing insecticide resistance in African malaria vectors. *Malaria Journal*, 15, 107. https://doi.org/10.1186/s12936-016-1162-4.

[105] Reyburn, H., Mbatia, R., Drakeley, C., Bruce, J., Carneiro, I., Olomi, R., and Riley, E. M. Association of transmission intensity and age with clinical manifestations and case fatality of severe *Plasmodium falciparum malaria* (2005). *JAMA*. **293**: 1461 -1470.

[106] Rickman, L.S., Jones, T.R., Long, G.W., Paparello, S., Schneider, I., Paul, C.F., and Hoffman, S. L. *Plasmodium falciparum*-infected *Anopheles stephensi* inconsistently transmit malaria to humans (1990). The *American Journal of Tropical Medicine and Hygiene*. **43**: 441-445.

[107] Sama, W., Killeen, G., and Smith, T. Estimating the duration of *Plasmodium falciparum* infection from trials of indoor residual spraying (2004). *The American Journal of Tropical Medicine and Hygiene*. **70**: 625-634.

[108] Smith D.L., Dushoff J., Snow R.W. and Hay S.I. The entomological inoculation rate and *Plasmodium falciparum* infection in African children (2005). *Nature*. **438**: 492-495.

[109] David L., Smith S.I., Hay A. M., Noor and Robert W.S.(2009). Predicting changing malaria risk after expanded insecticide-treated net coverage in Africa. *Trends Parasitol.* **25**(11): 511-516. doi: 10.1016/j.pt.2009.08.002

[110] Takken, W., Klowden, M. J., and Chambers, G. M. Effect of body size on host seeking and blood meal utilization in *Anopheles gambiae sensu stricto (Diptera: Culicidae)*: the disadvantage of being small (1998). *Journal of Medical Entomology*. 35: 639 - 645.

[111] The Alliance for Malaria Prevention. "Net Mapping Q2 2018". http://allianceformalariaprevention.com/net-mapping-project/

[112] Tobias *et al.*. The Effect of Insecticide Treated Nets (ITNs) on *Plasmodium falciparum* Infection in Rural and Semi-Urban Communities in the South West Region of Cameroon. *PLoS ONE* **10**(2): e0116300. doi:10.1371/journal.pone.0116300.

[113] K. H. Toe, P. MÃŒller, A. Badolo, A. Traore, N. Sagnon, R. K. Dabire, H. Ranson (2018). Do bednets including piperonyl butoxide offer additional protection against populations of Anopheles gambiae s.l. that are highly resistant to pyrethroids? An experimental hut evaluation in Burkina Faso. Medical and Veterinary Entomology. 32, 407–416.

[114] Tungu P., Magesa S., Maxwell C., Malima R., Masue D., Sudi W. and Rowland M. (2010). Evaluation of PermaNet 3.0 a deltamethrin-PBO combination net against *Anopheles gambiae* and pyrethroid resistant *Culex quinquefasciatus* mosquitoes: an experimental hut trial in Tanzania. *Malaria Journal*, **9**(1), 21.

[115] van den Driessche P. and Watmough J. (2002). Reproduction numbers and subthreshold endemic equilibria for compartmental models of disease transmission. *Math. Biosci.* **180**: 29-48.

[116] Yaro A.S., Dao A., Adamou A., Crawford J.E., Ribeiro J.M., Gwadz, R., *et al* (2006). The distribution of hatching time in *Anopheles gambiae*. *Malar. J.* 5: 19.

[117] https://www.gatesfoundation.org/What-We-Do/Global-Health/Malaria.

[118] Weidong G.u. and Robert J. Novak. Predicting the impact of insecticide-treated bed nets on malaria transmission: the devil is in the detail (2009). *Malaria Journal*. **8**: 256

[119] Willis, Derek W. and Hamon N. Eliminating malaria by 2040 among agricultural households in Africa; potential impact on health, labor productivity, education and gender equality. *Gates Open Research*. 2018, **2**:33 (https://doi.org/10.12688/gatesopenres.12843.2).

[120] World Health Organization. 2015. Malaria: Draft Global Technical Strategy. Sixty-Eighth World Health Assembly, March 20, 2015.

[121] World Health Organization. 2012. World Malaria Report 2012. Geneva, Switzerland.

[122] World Health Organization. 2015. World Malaria Report 2015. http://www.who.int/malaria/publications/world-malaria-report-2015/report/en/

[123] World Health Organization. 2015. Global Technical Strategy for Malaria 2016-2030. Retrieved from http://www.who.int/malaria/publications/atoz/9789241564991/en/

[124] World Health Organization. 2016. World Malaria Report 2016. http://apps.who.int/iris/bitstream/10665/252038/1/9789241511711-eng.pdf?ua=1.

[125] World Health Organization. 2017. Malaria Media Center:fact sheet, updated April 2017. http://www.who.int/mediacentre/factsheets/fs094/en/

[126] World Health Organization. 2017. Global Insecticide Resistance Database. November 2017. `https://www.who.int/malaria/areas/vector_control/en/`

[127] World Health Organization. Achieving and maintaining universal coverage with long-lasting insecticidal nets for malaria control, Ed., World Health Organization, Geneva, 2017.

[128] World Health Organization. Global technical strategy for malaria 2016-2030, Ed., World Health Organization, Geneva, 2015.

[129] World Health Organization. WHO recommended insecticides for indoor residual spraying against malaria vectors. https://www.who.int/neglected_diseases/vector_ecology/vector-control/Insecticides_IRS_22_September_2018.pdf?ua= 1. Accessed: April 6, 2019.

[130] World Health Organization. World Malaria Day 2018: Ready to beat malaria. https://www.who.int/malaria/media/world-malaria-day-2018/en/. Accessed: March 10, 2019.

Appendix A: Proof of Lemma 2.1

Proof. (a) It should be noted, first of all, that the right-hand side of each of the equations of the model {(2.1), (2.2),(2.4)} is continuous and locally-Lipschitz at $t = 0$. Hence, a solution of the model with non-negative initial conditions exists and is unique in $\Omega = \Omega_1 \times \Omega_2 \times \Omega_3$ for all time $t > 0$ (see also [61, 96]). Furthermore, since $\left(1 - \frac{E}{K_E}\right)_+ \geq 0$, it follows from the first equation of the sub-system (2.1) that $E(t) \leq K_E$ for all time $t > 0$. Similarly, it follows from the second equation of the sub-system (2.1) that

$$\dot{L}_1 = \sigma_E E - (\sigma_{L_1} + \mu_L) L_1 \leq \sigma_E K_E - (\sigma_{L_1} + \mu_L) L_1,$$

so that $\limsup_{t\to\infty} L_1(t) \leq \dfrac{\sigma_E K_E}{\sigma_{L_1} + \mu_L} = L_1^\diamond$. Using a similar approach, it can be shown that $\limsup_{t\to\infty} L_2(t) \leq \dfrac{\sigma_{L_1} L_1^\diamond}{\sigma_{L_2} + \mu_L} = L_2^\diamond$, $\limsup_{t\to\infty} L_3(t) \leq \dfrac{\sigma_{L_2} L_2^\diamond}{\sigma_{L_3} + \mu_L} = L_3^\diamond$, $\limsup_{t\to\infty} L_4(t) \leq \dfrac{\sigma_{L_3} L_3^\diamond}{\sigma_{L_4} + \mu_L} = L_4^\diamond$ and $\limsup_{t\to\infty} P(t) \leq \dfrac{\sigma_{L_4} L_4^\diamond}{\sigma_P + \mu_P} = P^\diamond$. That is, all solutions of the sub-system (2.1) are bounded for all time $t > 0$.

For the boundedness of the solutions of the sub-system (2.2), we consider the following equation (for the rate of change of the total adult mosquito population):

$$\dot{N}_M = f\sigma_P P - \mu_{\mathbf{X}} S_X - \mu_{\mathbf{X}} E_X - \mu_{\mathbf{X}} I_X - \mu_M N_M + b_H(Q_2 + Q_3 - Q_1 + R_1 + R_2) A_X, \quad \text{(A-1)}$$

where, $N_M = A_X + A_Y + A_Z$ (with $A_X, A_Y, A_Z, Q_1, Q_2, Q_3, R_1$ and R_2 are as defined in Section 2). It can be shown that $Q_2 + Q_3 - Q_1 + R_1 + R_2 < 0$. Hence, Equation (A-1) can be re-written as

$$\dot{N}_M = f\sigma_P P - \mu_{\mathbf{X}} S_X - \mu_{\mathbf{X}} E_X - \mu_{\mathbf{X}} I_X - \mu_M N_M + b_H(Q_2 + Q_3 - Q_1 + R_1 + R_2) A_X \leq f\sigma_P P - \mu_M N_M, \quad \text{(A-2)}$$

so that,

$$\limsup_{t\to\infty} N_M(t) \leq \frac{f\sigma_P P^\diamond}{\mu_M}.$$

Hence, the solutions of the equations of the sub-system (2.2) are bounded for all time $t > 0$. Similarly, consider the equation for the rate of change of the total human population, given by:

$$\dot{N}_H = \Pi - \mu_H N_H - \delta_H(I_{H_p} + I_{H_u}) \leq \Pi - \mu_H N_H, \quad \text{(A-3)}$$

from which it follows that $\limsup_{t\to\infty} N(t) \leq \dfrac{\Pi}{\mu_H}$. Thus, the solutions of the sub-system (2.4) are bounded for all $t > 0$. Since the solutions of the three sub-systems of the model {(2.1), (2.2),(2.4)} are bounded, it follows that the solutions of the model are bounded. This concludes the proof of Item (a).

(b) The proof for the invariance of the region Ω_1 follows from the bounds established in Item (a) (i.e., $0 < \limsup_{t\to\infty} L_1(t) \leq L_1^\diamond$, $0 < \limsup_{t\to\infty} L_j(t) \leq L_j^\diamond$ and $0 < \limsup_{t\to\infty} P(t) \leq P^\diamond$) and

the fact that $\dot{E}(t) < 0$ whenever $E(t) > K_E$, $\dot{L}_1(t) < 0$ whenever $L_1(t) > L_1^\diamond$ and $\dot{L}_j(t) < 0$ whenever $L_j(t) > L_1^\diamond$ $(j = 2, 3, 4)$, respectively.

For the invariance of the region Ω_2, it is convenient to consider the following equation for the rate of change of the total mosquito population given by:

$$\dot{N}_M = f\sigma_P P - \mu_{\mathbf{X}} S_X - \mu_{\mathbf{X}} E_X - \mu_{\mathbf{X}} I_X - \mu_M N_M + b_H(Q_2 + Q_3 - Q_1 + R_1 + R_2)A_X \leq f\sigma_P P - \mu_M N_M.$$

It follows that $\dot{N}_M < 0$ whenever $N_M(t) > \frac{f\sigma_P P^\diamond}{\mu_M}$. Thus, the region Ω_2 is invariant with respect to the sub-system (2.2) of the model $\{$(2.1), (2.2),(2.4)$\}$.

Finally, consider the equation for the total human population given by

$$\dot{N}_H = \Pi - \mu_H N_H - \delta_H(I_{Hp} + I_{Hu}) \leq \Pi - \mu_H N_H.$$

It follows that $\dot{N}_H < 0$ whenever $N_H(t) > \frac{\Pi}{\mu_H}$. Thus, the region Ω_3 is invariant with respect to the sub-system (2.4) of the model $\{$(2.1), (2.2),(2.4)$\}$. Since the regions Ω_1, Ω_2 and Ω_3 are positively-invariant and attracting, it follows that $\Omega = \Omega_1 \times \Omega_2 \times \Omega_3$ is positively-invariant and attracting for the model $\{$(2.1), (2.2),(2.4)$\}$. This concludes the proof of Item (b). □

Appendix B: Coefficients of Equation (3.5)

$$\begin{aligned}
C_1 &= b_H\left\{\pi_p(1-\varepsilon_{deter})[(1-\varepsilon_{die,p})\varepsilon_{bite|\sim die,p} + \varepsilon_{die,p}] + \pi_u[(1-\varepsilon_{die,u})\varepsilon_{bite|\sim die,u} + \varepsilon_{die,u}]\right\} + \mu_{\mathbf{X}} + \mu_M > 0,\\
C_2 &= b_H[\pi_p(1-\varepsilon_{deter})(1-\varepsilon_{die,p})\varepsilon_{bite|\sim die,p} + \pi_u(1-\varepsilon_{die,u})\varepsilon_{bite|\sim die,u}] > 0,\\
C_3 &= b_H\left\{\pi_p(1-\varepsilon_{deter})[(1-\varepsilon_{die,p})\varepsilon_{bite|\sim die,p} + \varepsilon_{die,p}] + \pi_u[(1-\varepsilon_{die,u})\varepsilon_{bite|\sim die,u} + \varepsilon_{die,u}]\right\} + \kappa_V + \mu_{\mathbf{X}} + \mu_M > 0,\\
C_4 &= \left\{\pi_p(1-\varepsilon_{deter})[\varepsilon_{die,p}(1-\varepsilon_{bite|\sim die,p}) + \varepsilon_{bite|\sim die,p}] + \pi_u[\varepsilon_{die,u}(1-\varepsilon_{bite|\sim die,u}) + \varepsilon_{bite|\sim die,u}]\right\}\kappa_V^2 > 0,\\
C_5 &= 2\kappa_V\left(\mu_M + \frac{\theta_Y}{2} + \frac{\varphi_Z}{2}\right)C_4 > 0,\\
C_6 &= \pi_p(1-\varepsilon_{deter})\left\{[\varepsilon_{die,p}(1-\varepsilon_{bite|\sim die,p}) + \varepsilon_{bite|\sim die,p}]\mu_M^2 + (\theta_Y+\varphi_Z)[\varepsilon_{die,u}(1-\varepsilon_{bite|\sim die,u}) + \varepsilon_{bite|\sim die,u}]\mu_M + \varepsilon_{bite|\sim die,p}\theta_Y\varphi_Z\right\} > 0,\\
C_7 &= \pi_u\left\{[\varepsilon_{die,u}(1-\varepsilon_{bite|\sim die,u}) + \varepsilon_{bite|\sim die,u}]\mu_M^2 + (\theta_Y+\varphi_Z)[\varepsilon_{die,u}(1-\varepsilon_{bite|\sim die,u}) + \varepsilon_{bite|\sim die,u}]\mu_M + \varepsilon_{bite|\sim die,u}\theta_Y\varphi_Z\right\} > 0,\\
C_8 &= (\mu_M + \kappa_V)K_{10}K_{12},\\
C_9 &= \varphi_Z + \theta_Y + b_H\left\{\pi_p(1-\varepsilon_{deter})[1-(1-\varepsilon_{die,p})(1-\varepsilon_{bite|\sim die,p})] + \pi_u[1-(1-\varepsilon_{die,u})(1-\varepsilon_{bite|\sim die,u})]\right\} > 0,\\
C_{10} &= \theta_Y\varphi_Z + b_H(\theta_Y+\varphi_Z)\left\{\pi_p(1-\varepsilon_{deter})[1-(1-\varepsilon_{die,p})(1-\varepsilon_{bite|\sim die,p})] + \pi_u[1-(1-\varepsilon_{die,u})(1-\varepsilon_{bite|\sim die,u})]\right\} > 0,\\
C_{11} &= b_H\theta_Y\varphi_Z[\pi_p\varepsilon_{die,p}(1-\varepsilon_{deter}) + \varepsilon_{die,u}\pi_u] > 0.
\end{aligned}$$

Appendix C: Equations of the Model {(2.1), (2.2), (2.4)} Without Bednets Intervention

In the absence of the bednet-based intervention, the sub-systems of the model involving the adults and human dynamics, given by Equations (2.2) and (2.4), reduce, respectively, to the following sub-systems:

$$\text{Stage I}\begin{cases}\dot{S}_X &= f\sigma_P P + \varphi_Z S_Z + b_H Q_3 S_X - (b_H + \mu_{\mathbf{X}} + \mu_M)\, S_X,\\ \dot{E}_X &= \varphi_Z E_Z + b_H Q_3 E_X - (b_H + \kappa_V + \mu_{\mathbf{X}} + \mu_M)\, E_X,\\ \dot{I}_X &= \varphi_Z I_Z + \kappa_V E_X + b_H Q_3 I_X - (b_H + \mu_{\mathbf{X}} + \mu_M)\, I_X.\end{cases}$$

$$\text{Stage II}\begin{cases}\dot{S}_Y &= (1-\beta_V\omega) R_2 S_X - (\theta_Y + \mu_M)\, S_Y,\\ \dot{E}_Y &= b_H\beta_V\omega R_2 S_X + b_H R_2 E_X - (\theta_Y + \kappa_V + \mu_M)\, E_Y,\\ \dot{I}_Y &= \kappa_V E_Y + b_H R_2 I_X - (\theta_Y + \mu_M)\, I_Y.\end{cases}$$

(C-1)

$$\text{Stage III}\begin{cases}\dot{S}_Z &= \theta_Y S_Y - (\varphi_Z + \mu_M)\, S_Z,\\ \dot{E}_Z &= \theta_Y E_Y - (\varphi_Z + \kappa_V + \mu_M)\, E_Z,\\ \dot{I}_Z &= \theta_Y I_Y + \kappa_V E_Z - (\varphi_Z + \mu_M)\, I_Z,\end{cases}$$

$$\text{Human}\begin{cases}\dot{S}_H &= \Pi - (\lambda_{VH} + \mu_H) S_H + \eta_H R_H,\\ \dot{E}_H &= \lambda_{VH} S_H - (\gamma_H + \mu_H) E_H,\\ \dot{I}_H &= \gamma_H E_H - (\alpha_H + \delta_H + \mu_H) I_H,\\ \dot{R}_H &= \alpha_H I_H - (\eta_H + \mu_H) R_H.\end{cases}$$

(C-2)

The equations for the aquatic dynamics, given by (2.1), remain unchanged. Hence, the reduced (no-bednets) model consist of the equations $\{(2.1), (C\text{-}1), (C\text{-}2)\}$.

It can be shown, using the next generation operator method (as in Section 3), that the basic reproduction number of the reduced model $\{(2.1), (C\text{-}1),\ (C\text{-}2)\}$ is given by

$$\tilde{\mathcal{R}}_{0*} = \sqrt{\frac{b_H\beta_V J_1 J_3 S_X^0 \beta_M \gamma_H \theta_Y \varphi_Z \kappa_V [(K_9 + K_{12})J_5 + K_9 K_{11}]}{K_{13}K_{14}N_H^*(J_5 K_{10} K_{12} - J_6\theta_Y\varphi_Z)(J_4 K_9 K_{11} - J_6\theta_Y\varphi_Z)}}, \tag{C-3}$$

where,

$$J_1 = b_H\left[\varepsilon_{bite|die,u}\,\varepsilon_{die,u} + \varepsilon_{bite|\sim die,u}(1-\varepsilon_{die,u})\right],\ J_2 = (1-\varepsilon_{die,u})(1-\varepsilon_{bite|\sim die,u}),\ N_H^* = \frac{\Pi}{\mu_H},$$
$$J_3 = (1-\varepsilon_{die,u})\varepsilon_{bite|\sim die,u},\ J_4 = (b_H + \mu_{\mathbf{X}} + \mu_M) - b_H J_2,\ J_5 = (b_H + \kappa_V + \mu_{\mathbf{X}} + \mu_M) - b_H J_2,$$
$$J_6 = b_H J_3,\ \mathcal{N}_{0*} = \frac{(\psi_E\varphi_Z\sigma_E f\sigma_P\theta_Y J_6)\prod_{i=1}^{4}\sigma_{L_i}}{(J_4K_9K_{11} - J_6\theta_Y\varphi_Z)\prod_{i=1}^{6}K_i},\ S_X^0 = \frac{\left[f\sigma_E\sigma_P K_E\left(1-\frac{1}{\mathcal{N}_{0*}}\right)K_9K_{11}\right]\prod_{i=1}^{4}\sigma_{L_i}}{(J_4K_9K_{11} - J_6\theta_Y\varphi_Z)\prod_{i=2}^{6}K_i}.$$

Substituting the baseline parameter values in Table 4 (for the holo-endemic setting) shows that the worst-case scenario basic reproduction number ($\tilde{\mathcal{R}}_0$) of the model $\{(2.1), (2.2), (2.4)\}$, or, equivalently, the reduced model $\{(C\text{-}1), (C\text{-}2)\}$, given by (C-3), is $\tilde{\mathcal{R}}_{0*} = \mathbf{11.4}$.

Appendix D: Proof of Theorem 3.2

Proof. The proof of Theorem 3.2 is based on using center manifold theory [23, 24]. It is convenient to define the following change of variables for the model {(2.1), (2.2), (2.4)}: $E = x_1$, $L_1 = x_2$, $L_2 = x_3$, $L_3 = x_4$, $L_4 = x_5$, $P = x_6$, $S_X = x_7$, $E_X = x_8$, $I_X = x_9$, $S_Y = x_{10}$, $E_Y = x_{11}$, $I_Y = x_{12}$, $S_Z = x_{13}$, $E_Z = x_{14}$, $I_Z = x_{15}$, $S_{Hp} = x_{16}$, $E_{Hp} = x_{17}$, $I_{Hp} = x_{18}$, $R_{Hp} = x_{19}$, $S_{Hu} = x_{20}$, $E_{Hu} = x_{21}$, $I_{Hu} = x_{22}$, $R_{Hu} = x_{23}$. Using the vector notation $X = (x_1, ...x_{23})^T$ and $F = (f_1, ...f_{23})^T$, the model can then be written in the form $\frac{dX}{dt} = (f_1, ...f_{23})^T$, as follows:

$$
\begin{aligned}
\dot{x}_1 \equiv f_1 &= \psi_E \varphi_Z \left(1 - \frac{x_1}{K_E}\right)_+ (x_{13} + x_{14} + x_{15}) - (\sigma_E + \mu_E)\, x_1,\\
\dot{x}_2 \equiv f_2 &= \sigma_E x_1 - (\sigma_{L_1} + \mu_L)\, x_2,\\
\dot{x}_3 \equiv f_3 &= \sigma_{L_1} x_2 - (\sigma_{L_2} + \mu_L)\, x_3,\\
\dot{x}_4 \equiv f_4 &= \sigma_{L_2} x_3 - (\sigma_{L_3} + \mu_L)\, x_4,\\
\dot{x}_5 \equiv f_5 &= \sigma_{L_3} x_4 - (\sigma_{L_4} + \mu_L)\, x_5,\\
\dot{x}_6 \equiv f_6 &= \sigma_{L_4} x_5 - (\sigma_P + \mu_P)\, x_6,\\
\dot{x}_7 \equiv f_7 &= f\sigma_P x_6 + \varphi_Z x_{13} + b_H(Q_2 + Q_3)x_7 - (b_H Q_1 + \mu_X + \mu_M)\, x_7,\\
\dot{x}_8 \equiv f_8 &= \varphi_Z x_{14} + b_H(Q_2 + Q_3)x_8 - (b_H Q_1 + \kappa_V + \mu_X + \mu_M)\, x_8,\\
\dot{x}_9 \equiv f_9 &= \varphi_Z x_{15} + \kappa_V x_8 + b_H(Q_2 + Q_3)x_9 - (b_H Q_1 + \mu_X + \mu_M)\, x_9,\\
\dot{x}_{10} \equiv f_{10} &= b_H[(1 - \beta_V\omega_p)R_1 + (1 - \beta_V\omega_u)R_2]x_7 - (\theta_Y + \mu_M)\, x_{10},\\
\dot{x}_{11} \equiv f_{11} &= b_H(\beta_V\omega_p R_1 + \beta_V\omega_u R_2)x_7 + b_H(R_1 + R_2)x_8 - (\theta_Y + \kappa_V + \mu_M)\, x_{11},\\
\dot{x}_{12} \equiv f_{12} &= \kappa_V x_{11} + b_H(R_1 + R_2)x_9 - (\theta_Y + \mu_M)\, x_{12},\\
\dot{x}_{13} \equiv f_{13} &= \theta_Y x_{10} - (\varphi_Z + \mu_M)\, x_{13},\\
\dot{x}_{14} \equiv f_{14} &= \theta_Y x_{11} - (\varphi_Z + \kappa_V + \mu_M)\, x_{14},\\
\dot{x}_{15} \equiv f_{15} &= \theta_Y x_{12} + \kappa_V x_{14} - (\varphi_Z + \mu_M)\, x_{15},\\
\dot{x}_{16} \equiv f_{20} &= \Pi\pi_p - (\lambda_{VH_p} + \mu_H)x_{16} + \eta_H x_{19},\\
\dot{x}_{17} \equiv f_{21} &= \lambda_{VH_p} x_{16} - (\gamma_H + \mu_H)x_{17},\\
\dot{x}_{18} \equiv f_{22} &= \gamma_H x_{17} - (\alpha_H + \delta_H + \mu_H)x_{18},\\
\dot{x}_{19} \equiv f_{23} &= \alpha_H x_{18} - (\eta_H + \mu_H)x_{19},\\
\dot{x}_{20} \equiv f_{24} &= \Pi\pi_u - (\lambda_{VH_u} + \mu_H)x_{20} + \eta_H x_{23},\\
\dot{x}_{21} \equiv f_{25} &= \lambda_{VH_u} x_{20} - (\gamma_H + \mu_H)x_{21},\\
\dot{x}_{22} \equiv f_{26} &= \gamma_H x_{21} - (\alpha_H + \delta_H + \mu_H)x_{22},\\
\dot{x}_{23} \equiv f_{27} &= \alpha_H x_{22} - (\eta_H + \mu_H)x_{23},
\end{aligned}
\tag{D-1}
$$

where,

$$\begin{aligned}
\mathrm{EIR}_p &= b_H \frac{x_9}{N_{H_p}} \pi_p (1-\varepsilon_{deter}) \left[\varepsilon_{bite|die,p}\varepsilon_{die,p} + \epsilon_{bite|\sim die,p}(1-\varepsilon_{die,p})\right], \\
\mathrm{EIR}_u &= b_H \frac{x_9}{N_{H_u}} \pi_u \left[\varepsilon_{bite|die,u}\varepsilon_{die,u} + \varepsilon_{bite|\sim die,u}(1-\varepsilon_{die,u})\right], \\
\lambda_{VH_p} &= \beta_M \,\mathrm{EIR}_p, \\
\lambda_{VH_u} &= \beta_M \,\mathrm{EIR}_u, \\
\omega_p &= \frac{x_{18}}{N_{H_p}},\ \omega_u = \frac{x_{22}}{N_{H_u}}.
\end{aligned}$$

Let $\mathcal{R}_0 = 1$ and suppose, further, that $\beta_M = \beta_M^*$ is chosen as a bifurcation parameter. Solving for $\beta_M = \beta_M^*$ from $\mathcal{R}_0 = 1$ gives

$$\beta_M = \beta_M^* = \frac{\Pi \pi_p \pi_u \left(C_3K_{10}K_{12} - C_2\theta_Y\varphi_Z\right)\left(C_1K_9K_{11} - C_2\theta_Y\varphi_Z\right)}{\mu_H^2 b_H x_7^* \kappa_V \varphi_Z \theta_Y [(K_9+K_{12})C_3 + K_9K_{11}](\mathcal{R}_{H_pV} + \mathcal{R}_{H_uV})}.$$

The Jacobian of the transformed system (D-1), evaluated at the DFE ($\mathcal{T}_2$) with $\beta_M = \beta_M^*$, is given by

$$J(\beta_M^*) = \begin{bmatrix} J_1 & J_2 \\ J_3 & J_4 \end{bmatrix},$$

where,

$$J_1 = \begin{bmatrix}
-\frac{\psi_E\varphi_Z x_{13}^*}{K_E} - K_1 & 0 & 0 & 0 & 0 & 0 & 0 & 0 & 0 & 0 & 0 & 0 \\
\sigma_E & -K_2 & 0 & 0 & 0 & 0 & 0 & 0 & 0 & 0 & 0 & 0 \\
0 & \sigma_{L_1} & -K_3 & 0 & 0 & 0 & 0 & 0 & 0 & 0 & 0 & 0 \\
0 & 0 & \sigma_{L_2} & -K_4 & 0 & 0 & 0 & 0 & 0 & 0 & 0 & 0 \\
0 & 0 & 0 & \sigma_{L_3} & -\mu_H & 0 & 0 & 0 & 0 & 0 & 0 & 0 \\
0 & 0 & 0 & 0 & \sigma_{L_4} & -K_5 & 0 & 0 & 0 & 0 & 0 & 0 \\
0 & 0 & 0 & 0 & 0 & f\sigma_P & -C_1 & 0 & 0 & 0 & 0 & 0 \\
0 & 0 & 0 & 0 & 0 & 0 & 0 & -C_3 & 0 & 0 & 0 & 0 \\
0 & 0 & 0 & 0 & 0 & 0 & 0 & \kappa_V & -C_1 & 0 & 0 & 0 \\
0 & 0 & 0 & 0 & 0 & 0 & C_2 & 0 & 0 & -K_9 & 0 & 0 \\
0 & 0 & 0 & 0 & 0 & 0 & 0 & C_2 & 0 & 0 & -K_{10} & 0 \\
0 & 0 & 0 & 0 & 0 & 0 & 0 & 0 & C_2 & 0 & \kappa_V & -K_9
\end{bmatrix},$$

$$J_2 = \begin{bmatrix}
\psi_E\varphi_Z(1-\frac{x_1^*}{K_E}) & \psi_E\varphi_Z(1-\frac{x_1^*}{K_E}) & \psi_E\varphi_Z(1-\frac{x_1^*}{K_E}) & 0 & 0 & 0 & 0 & 0 & 0 & 0 & 0 \\
0 & 0 & 0 & 0 & 0 & 0 & 0 & 0 & 0 & 0 & 0 \\
0 & 0 & 0 & 0 & 0 & 0 & 0 & 0 & 0 & 0 & 0 \\
0 & 0 & 0 & 0 & 0 & 0 & 0 & 0 & 0 & 0 & 0 \\
0 & 0 & 0 & 0 & 0 & 0 & 0 & 0 & 0 & 0 & 0 \\
0 & 0 & 0 & 0 & 0 & 0 & 0 & 0 & 0 & 0 & 0 \\
\varphi_Z & 0 & 0 & 0 & 0 & 0 & 0 & 0 & 0 & 0 & 0 \\
0 & \varphi_Z & 0 & 0 & 0 & 0 & 0 & 0 & 0 & 0 & 0 \\
0 & 0 & \varphi_Z & 0 & 0 & 0 & 0 & 0 & 0 & 0 & 0 \\
0 & 0 & 0 & 0 & 0 & -\frac{b_H R_1 \beta_V x_7^*}{x_{16}^*} & 0 & 0 & 0 & -\frac{b_H R_2 \beta_V x_7^*}{x_{20}^*} & 0 \\
0 & 0 & 0 & 0 & 0 & \frac{b_H R_1 \beta_V x_7^*}{x_{16}^*} & 0 & 0 & 0 & \frac{b_H R_2 \beta_V x_7^*}{x_{20}^*} & 0 \\
0 & 0 & 0 & 0 & 0 & 0 & 0 & 0 & 0 & 0 & 0
\end{bmatrix},$$

$$J_3 = \begin{bmatrix} 0 & 0 & 0 & 0 & 0 & 0 & 0 & 0 & \theta_Y & 0 & 0 \\ 0 & 0 & 0 & 0 & 0 & 0 & 0 & 0 & 0 & \theta_Y & 0 \\ 0 & 0 & 0 & 0 & 0 & 0 & 0 & 0 & 0 & 0 & \theta_Y \\ 0 & 0 & 0 & 0 & 0 & 0 & 0 & -\beta_M Q_p & 0 & 0 & 0 \\ 0 & 0 & 0 & 0 & 0 & 0 & 0 & \beta_M Q_p & 0 & 0 & 0 \\ 0 & 0 & 0 & 0 & 0 & 0 & 0 & 0 & 0 & 0 & 0 \\ 0 & 0 & 0 & 0 & 0 & 0 & 0 & 0 & 0 & 0 & 0 \\ 0 & 0 & 0 & 0 & 0 & 0 & 0 & -\beta_M Q_u & 0 & 0 & 0 \\ 0 & 0 & 0 & 0 & 0 & 0 & 0 & \beta_M Q_u & 0 & 0 & 0 \\ 0 & 0 & 0 & 0 & 0 & 0 & 0 & 0 & 0 & 0 & 0 \\ 0 & 0 & 0 & 0 & 0 & 0 & 0 & 0 & 0 & 0 & 0 \end{bmatrix},$$

and,

$$J_4 = \begin{bmatrix} -K_{11} & 0 & 0 & 0 & 0 & 0 & 0 & 0 & 0 & 0 & 0 \\ 0 & -K_{12} & 0 & 0 & 0 & 0 & 0 & 0 & 0 & 0 & 0 \\ 0 & \kappa_V & -K_{11} & 0 & 0 & 0 & 0 & 0 & 0 & 0 & 0 \\ 0 & 0 & 0 & -\mu_H & 0 & 0 & \eta_H & 0 & 0 & 0 & 0 \\ 0 & 0 & 0 & 0 & -K_{13} & 0 & 0 & 0 & 0 & 0 & 0 \\ 0 & 0 & 0 & 0 & \gamma_H & -K_{14} & 0 & 0 & 0 & 0 & 0 \\ 0 & 0 & 0 & 0 & 0 & \alpha_H & -K_{15} & 0 & 0 & 0 & 0 \\ 0 & 0 & 0 & 0 & 0 & 0 & 0 & -\mu_H & 0 & 0 & \eta_H \\ 0 & 0 & 0 & 0 & 0 & 0 & 0 & 0 & -K_{13} & 0 & 0 \\ 0 & 0 & 0 & 0 & 0 & 0 & 0 & 0 & \gamma_H & -K_{14} & 0 \\ 0 & 0 & 0 & 0 & 0 & 0 & 0 & 0 & 0 & \alpha_H & -K_{15} \end{bmatrix}.$$

The Jacobian $J(\beta_M^*)$ has a simple zero eigenvalue (and all other eigenvalues having negative real parts). Hence, the center manifold theory [23, 24] can be used to analyse the dynamics of (D-1) near $\beta_M = \beta_M^*$. This entails carrying out the following computations.

Eigenvectors of $J(\mathcal{T}_2)\,|_{\beta_M=\beta_M^*}$: The Jacobian of the transformed system (D-1), evaluated at the DFE ($\mathcal{T}_2$) with $\beta_M = \beta_M^*$, has a right and left eigenvectors (associated with the zero eigenvalue) (the expression for the eigenvector w_i and v_i, $i = 1, 2, .., 23$, are given in the Supplementary Material).

Computations of bifurcation coefficients of a **and** b :

By computing the associated non-zero partial derivatives of $F(x)$ evaluated the the DFE, it follows from Theorem 4.1 in [24] that the associated bifurcation coefficients, a and b, are given, respectively, by

$$\begin{aligned} a =& -2b_H \left[\frac{(-w_{22}R_2w_7v_{11}\beta_V + v_{21}Q_u\beta_M w_9(w_{22}+w_{21}+w_{23}))x_{20}^* + w_{22}\beta_V R_2 x_7^* v_{11}(w_{20}+w_{21}+w_{22}+w_{23})}{(x_{20}^*)^2} \right] \\ & -2b_H \left[\frac{(-w_{18}\beta_V R_1 w_7 v_{11} + Q_p\beta_M w_9(w_{18}+w_{19}+1))x_{16}^* + w_{18}(x_{20}^*)^2\beta_V R_1 x_7^* v_{11}(w_{16}+w_{18}+w_{19}+1)}{(x_{16}^*)^2} \right], \end{aligned} \tag{D-2}$$

and,

$$b = b_H w_9 \left(Q_u v_{21} + Q_p\right) > 0. \tag{D-3}$$

Hence, it follows from Theorem 4.1 of [24] that the transformed model (D-1) undegoes a backward bifurcation at $\mathcal{R}_0 = 1$ if the bifurcation coefficient a (given by (D-2)) is positive. This concludes the proof. □

Appendix E: Proof of Theorem 3.3.

Proof. Consider the special case of the model {(2.1), (2.2), (2.4)} without disease-induced mortality in the host population (i.e., $\delta_H = 0$). Further, let $\mathcal{N}_0 > 1$ (so that the NDFE, $\mathcal{T}_2$, exists) and $\tilde{\mathcal{R}}_0 \leq 1$. Setting $\delta_H = 0$ in the model {(2.1), (2.2), (2.4)} gives $N_H(t) \to \frac{\Pi}{\mu_H}$ as $t \to \infty$, and $\bar{K}_{14} = \alpha_H + \mu_H$. Hence, from now on, $N_H(t)$ is replaced by its limiting value, $\frac{\Pi}{\mu_H}$. Furthermore, consider the following linear Lyapunov function:

$$\mathcal{F} = g_1 E_{Hp} + g_2 I_{Hp} + g_3 E_{Hu} + g_4 I_{Hu} + g_5 E_X + g_6 I_X + g_7 E_Y + g_8 I_Y + g_9 E_Z + g_{10} I_Z,$$

where,

$$\begin{aligned}
g_1 &= \beta_V N_{Hu} \gamma_H b_H R_1 S_X \kappa_V \varphi_Z \theta_Y \left(C_3 \left(K_9 + K_{12}\right) + K_9 K_{11}\right), \\
g_2 &= \beta_V N_{Hu} b_H R_1 S_X \kappa_V \varphi_Z \theta_Y \left(C_3 \left(K_9 + K_{12}\right) + K_9 K_{11}\right) K_{13}, \\
g_3 &= \beta_V N_{Hp} \gamma_H b_H R_2 S_X \kappa_V \varphi_Z \theta_Y \left(C_3 \left(K_9 + K_{12}\right) + K_9 K_{11}\right), \\
g_4 &= \beta_V N_{Hp} b_H R_2 S_X \kappa_V \varphi_Z \theta_Y \left(C_3 \left(K_9 + K_{12}\right) + K_9 K_{11}\right) K_{13}, \\
g_5 &= \frac{C_2 \beta_M \gamma_H \theta_Y^2 \varphi_Z^2 \kappa_V^2 S_X \beta_V \left(C_3 \left(K_9 + K_{12}\right) + K_9 K_{11}\right)^2 \left(N_{Hp} Q_u R_2 S_{Hu} + N_{Hu} Q_p R_1 S_{Hp}\right)}{\left(C_3 K_{10} K_{12} - C_2 \theta_Y \varphi_Z\right) \left(C_1 K_9 K_{11} - C_2 \theta_Y \varphi_Z\right) C_3} \\
&\quad + \frac{K_9 K_{11} K_{13} \bar{K}_{14} N_{Hp} N_{Hu} \left(C_3 K_{10} K_{12} - C_2 \theta_Y \varphi_Z\right) \kappa_V}{C_3}, \\
g_6 &= K_9 K_{11} K_{13} \bar{K}_{14} N_{Hp} N_{Hu} \left(C_3 K_{10} K_{12} - C_2 \theta_Y \varphi_Z\right), \\
g_7 &= \frac{\beta_M \gamma_H \theta_Y^2 \varphi_Z^2 \kappa_V^2 S_X \beta_V \left(C_3 \left(K_9 + K_{12}\right) + K_9 K_{11}\right)^2 \left(N_{Hp} Q_u R_2 S_{Hu} + N_{Hu} Q_p R_1 S_{Hp}\right)}{\left(C_3 K_{10} K_{12} - C_2 \theta_Y \varphi_Z\right) \left(C_1 K_9 K_{11} - C_2 \theta_Y \varphi_Z\right)}, \\
g_8 &= \theta_Y K_{13} \bar{K}_{14} \varphi_Z N_{Hp} N_{Hu} \left(C_3 K_{10} K_{12} - C_2 \theta_Y \varphi_Z\right), \\
g_9 &= \frac{C_2 \beta_M \gamma_H \theta_Y^2 \varphi_Z^3 \kappa_V^2 S_X \beta_V \left(C_3 \left(K_9 + K_{12}\right) + K_9 K_{11}\right)^2 \left(N_{Hp} Q_u R_2 S_{Hu} + N_{Hu} Q_p R_1 S_{Hp}\right)}{\left(C_3 K_{10} K_{12} - C_2 \theta_Y \varphi_Z\right) \left(C_1 K_9 K_{11} - C_2 \theta_Y \varphi_Z\right) K_{12} C_3} \\
&\quad + \frac{\varphi_Z K_9 K_{13} \bar{K}_{14} N_{Hp} N_{Hu} \left(C_3 K_{10} K_{12} - C_2 \theta_Y \varphi_Z\right) \kappa_V \left(K_{11} + C_3\right)}{K_{12} C_3}, \\
\text{and, } g_{10} &= \varphi_Z K_9 K_{13} \bar{K}_{14} N_{Hp} N_{Hu} \left(C_3 K_{10} K_{12} - C_2 \theta_Y \varphi_Z\right).
\end{aligned}$$

The Lyapunov derivative of $\mathcal{F}$ (where a dot represents differentiation with respect to t) is

given by:

$$
\begin{aligned}
\dot{\mathcal{F}} &= g_1\dot{E}_{Hp} + g_2\dot{I}_{Hp} + g_3\dot{E}_{Hu} + g_4\dot{I}_{Hu} + g_5\dot{E}_X + g_6\dot{I}_X + g_7\dot{E}_Y + g_8\dot{I}_Y + g_9\dot{E}_Z + g_{10}\dot{I}_Z,\\
&= g_1(\lambda_{VH_p}S_{H_p} - K_{13}E_{H_p}) + g_2(\gamma_H E_{H_p} - \bar{K}_{14}I_{H_p}) + g_3(\lambda_{VH_u}S_{H_u} - K_{13}E_{H_u})\\
&+ g_4(\gamma_H E_{H_u} - \bar{K}_{14}I_{Hu}) + g_5(\varphi_Z E_Z - C_3E_X) + g_6(\varphi_Z I_Z + \kappa_V E_X - C_1I_X)\\
&+ g_7[(b_H\beta_V\omega_p R_1 + b_H\beta_V\omega_u R_2)S_X + C_2E_X - K_{10}E_Y] + g_8(\kappa_V E_Y + C_2I_X - K_9I_Y)\\
&+ g_9(\theta_Y E_Y - K_{12}E_Z) + g_{10}(\theta_Y I_Y + \kappa_V E_Z - K_{11}I_Z),\\
&= \left(\frac{g_1\beta_M Q_p S_{Hp}}{N_{Hp}} + \frac{g_3\beta_M Q_u S_{Hu}}{N_{Hu}} - g_6C_1 + g_8C_2\right)I_X + \left(\frac{g_7b_H\beta_V R_1S_X}{N_{Hp}} - g_2\bar{K}_{14}\right)I_{Hp}\\
&+ \left(\frac{g_7b_H\beta_V R_2S_X}{N_{Hu}} - g_4\bar{K}_{14}\right)I_{Hu} + (-g_1K_{13} + g_2\gamma_H)\,E_{Hp} + (-g_3K_{13} + g_4\gamma_H)\,E_{Hu}\\
&+ (-g_5C_3 + g_6\kappa_V + g_7C_2)\,E_X + (-g_7K_{10} + g_8\kappa_V + g_9\theta_Y)\,E_Y + (-g_9K_{12} + g_{10}\kappa_V + g_5\varphi_Z)\,E_Z\\
&+ (-g_8K_9 + g_{10}\theta_Y)I_Y + (-g_{10}K_{11} + g_6\varphi_Z)I_Z.
\end{aligned}
$$

Since $S_{Hp}(t) \leq N_{Hp}$, $S_{Hu}(t) \leq N_{Hu}$, $N_{Hp}(t) = \frac{\Pi\,\pi_p}{\mu_H}$ and $N_{Hu}(t) = \frac{\Pi\,\pi_u}{\mu_H}$ in Ω for all $t > 0$, it follows that:

$$
\begin{aligned}
\dot{\mathcal{F}} =& \leq K_{13}\bar{K}_{14}N_{Hp}N_{Hu}(C_1K_9K_{11} - C_2\theta_Y\varphi_Z)(C_3K_{10}K_{12} - C_2\theta_Y\varphi_Z)(\tilde{\mathcal{R}}_0^2 - 1)I_X\\
&+ \beta_V N_{Hu}b_H R_1S_X\kappa_V\varphi_Z\theta_Y\left(C_3\left(K_9 + K_{12}\right) + K_9K_{11}\right)K_{13}K_{14}(\tilde{\mathcal{R}}_0^2 - 1)I_{Hp}\\
&+ \beta_V N_{Hp}b_H R_2S_X\kappa_V\varphi_Z\theta_Y\left(C_3\left(K_9 + K_{12}\right) + K_9K_{11}\right)K_{13}K_{14}(\tilde{\mathcal{R}}_0^2 - 1)I_{Hu}\\
&+ \frac{\varphi_Z^2\left(N_{Hp}Q_uR_2S_{Hu} + N_{Hu}Q_pR_1S_{Hp}\right)\kappa_V^2\beta_V(C_3(K_9+K_{12}) + K_9K_{11})^2\theta_Y^2S_X\gamma_H\beta_M}{b_HK_{12}C_3(C_1K_9K_{11} - C_2\theta_Y\varphi_Z)}\left(1 - \frac{1}{\tilde{\mathcal{R}}_0^2}\right)E_Y.
\end{aligned}
$$

Hence, $\dot{\mathcal{F}} \leq 0$ if $\tilde{\mathcal{R}}_0 < 1$ with $\dot{\mathcal{F}} = 0$ if and only if $I_X = I_{Hp} = I_{Hu} = E_Y = 0$. Therefore, $\mathcal{F}$ is a Lyapunov function in Ω and it follows from LaSalle's Invariance Principle [75] that every solution to the equations in {(2.1), (2.2), (2.4)} (with $\delta_H = 0$ and initial conditions in Ω) converges to $\mathcal{T}_2$ as $t \to \infty$ That is,

$$
\begin{aligned}
&(E_X(t), I_X(t), E_Y(t), I_Y(t), E_Z(t), I_Z(t), E_{Hp}(t), I_{Hp}(t), R_{Hp}(t), E_{Hu}(t), I_{Hu}(t), R_{Hu}(t))\\
&\to (0,0,0,0,0,0,0,0,0,0,0,0) \text{ as } t \to \infty.
\end{aligned}
$$

$$
\text{Thus, } \mathcal{X}(t) \to \left(E^*, L_1^*, L_2^*, L_3^*, L_4^*, P^*, S_X^*, 0, 0, S_Y^*, 0, 0, S_Z^*, 0, 0, \frac{\Pi\,\pi_p}{\mu_H}, 0, 0, 0, \frac{\Pi\,\pi_u}{\mu_H}, 0, 0, 0\right)
$$

as $t \to \infty$ for $\tilde{\mathcal{R}}_0 \leq 1$. Hence, the NDFE, $\mathcal{T}_2$, is globally-asymptotically stable in Ω if $\tilde{\mathcal{R}}_0 \leq 1$ for the special case of the model {(2.1), (2.2), (2.4)} with $\delta_H = 0$. This completes the proof. □